ELSEVIER

Contents lists available at ScienceDirect

### **Mathematical Biosciences**

journal homepage: www.elsevier.com/locate/mbs



Original Research Article

## NREM–REM alternation complicates transitions from napping to non-napping behavior in a three-state model of sleep–wake regulation



Christina Athanasouli <sup>a,\*</sup>, Kelsey Kalmbach <sup>c</sup>, Victoria Booth <sup>a,b</sup>, Cecilia G. Diniz Behn <sup>c,d</sup>

- <sup>a</sup> Department of Mathematics University of Michigan, 530 Church Street, Ann Arbor, MI, 48109, USA
- b Department of Anesthesiology, University of Michigan, 1500 E Medical Center Drive, Ann Arbor, 48109-5048, MI, USA
- c Department of Applied Mathematics and Statistics Colorado School of Mines, 1500 Illinois Street, Golden, 80401. CO. USA
- d Department of Pediatrics, University of Colorado Anschutz Medical Campus, 13001 East 17th Place, Aurora, 80045, CO, USA

### ARTICLE INFO

# Keywords: Sleep-wake regulation Rapid Eye Movement (REM) sleep Non-REM (NREM) sleep NREM-REM alternation Circle maps Bifurcations Piecewise-smooth systems

### ABSTRACT

The temporal structure of human sleep changes across development as it consolidates from the polyphasic sleep of infants to the single nighttime sleep episode typical in adults. Experimental studies have shown that changes in the dynamics of sleep need may mediate this developmental transition in sleep patterning, however, it is unknown how sleep architecture interacts with these changes. We employ a physiologicallybased mathematical model that generates wake, rapid eye movement (REM) and non-REM (NREM) sleep states to investigate how NREM-REM alternation affects the transition in sleep patterns as the dynamics of the homeostatic sleep drive are varied. To study the mechanisms producing these transitions, we analyze the bifurcations of numerically-computed circle maps that represent key dynamics of the full sleep-wake network model by tracking the evolution of sleep onsets across different circadian (~ 24 h) phases. The maps are non-monotonic and discontinuous, being composed of branches that correspond to sleep-wake cycles containing distinct numbers of REM bouts. As the rates of accumulation and decay of the homeostatic sleep drive are varied, we identify the bifurcations that disrupt a period-adding-like behavior of sleep patterns in the transition between biphasic and monophasic sleep. These bifurcations include border collision and saddle-node bifurcations that initiate new sleep patterns, period-doubling bifurcations leading to higher-order patterns of NREM-REM alternation, and intervals of bistability of sleep patterns with different NREM-REM alternations. Furthermore, patterns of NREM-REM alternation exhibit variable behaviors in different regimes of constant sleep-wake patterns. Overall, the sequence of sleep-wake behaviors, and underlying bifurcations, in the transition from biphasic to monophasic sleep in this three-state model is more complex than behavior observed in models of sleep-wake regulation that do not consider the dynamics of NREM-REM alternation. These results suggest that interactions between the dynamics of the homeostatic sleep drive and the dynamics of NREM-REM alternation may contribute to the wide interindividual variation observed when young children transition from napping to non-napping behavior.

### 1. Introduction

In humans, rapid eye movement (REM) and non-REM (NREM) sleep regularly alternate across the sleep episode [1]. Data indicate that this ultradian (recurring with a period less than 24 h) NREM-REM alternation interacts with developmentally-mediated changes in sleep in early childhood [2]. However, the dynamical mechanisms of these interactions are not well understood. In this study, we use physiologically-based mathematical modeling to determine how NREM-REM alternation affects the transition between polyphasic and monophasic sleep

that represents a child's transition from napping to non-napping behavior

Sleep timing is primarily governed by interactions between circadian (~24 h) and homeostatic sleep drives, and their actions on neuronal sleep—wake regulatory networks, namely the networks of brainstem and hypothalamic neuronal populations that produce distinct states of wake, NREM sleep, and REM sleep [3,4]. Although the time scales of circadian and homeostatic sleep processes may vary with ontogeny or phylogeny, many features of these drives are conserved across both developmental stages and mammalian species.

<sup>🛱</sup> This work was funded by the National Science Foundation under grants DMS 1853506 (C.A. and V.B.) and DMS 1853511 (K.K. and C.D.B.).

<sup>\*</sup> Correspondence to: School of Mathematics, Georgia Institute of Technology, 686 Cherry St NW, Atlanta, 30332, GA, USA.

E-mail addresses: chrath@umich.com (C. Athanasouli), kelsey.kalmbach@gmail.com (K. Kalmbach), vbooth@umich.com (V. Booth), cdinizbe@mines.com (C.G. Diniz Behn).

The circadian regulation of sleep is driven by projections from the circadian pacemaker in the suprachiasmatic nucleus (SCN) to the sleep—wake regulatory network [4,5]. In SCN neurons, intrinsic molecular clocks with periods of approximately 24 h are entrained to the 24 h light–dark cycle and produce daily oscillations in firing rate [6,7]. Projections from the SCN to downstream neuronal populations coordinate biological rhythms throughout the body and rhythmically modify sleep propensity, producing nocturnal, diurnal, crepuscular, or other sleep patterns (reviewed in [4]).

The homeostatic sleep drive increases with time awake, reflecting sleep need with a dependence on the past history of time spent in sleep and wakefulness. It is likely mediated by many mechanisms, including the somnogen adenosine [8–10]. Slow wave activity (SWA) in the electroencephalogram (EEG) is an established marker of the homeostatic sleep drive [11,12], and sleep deprivation experiments have been used to estimate the time constants associated with the homeostatic sleep drive in adults with typical sleep—wake behavior [13] as well as in humans in other life stages [14–16], and in other mammalian species [17,18].

The circadian and homeostatic sleep drives additionally influence NREM–REM alternation during a sleep episode. In adults, the circadian rhythm strongly modulates the occurrence of REM sleep, and there is a lower propensity for entering the REM state at phases when the circadian waking drive is high [19,20]. Similarly, high homeostatic sleep drive affects REM sleep by preferentially promoting NREM sleep over REM sleep during initial recovery sleep following sleep deprivation [20,21]. Total amounts of REM and NREM sleep also differ with sleep duration as reported in studies of habitually short- and long-sleeping individuals [15,22,23].

Across the human lifespan, the sleep–wake regulatory network produces a range of sleep behaviors, including frequent transitions between sleep and wake states in infants, regular napping behavior in early childhood, and a consolidated nighttime sleep episode in adults [24]. These ontogenetic changes are likely driven by changing dynamics of the homeostatic sleep drive, and experiments have identified differences in the rates of growth and decay of SWA in humans at different life stages [14,16,25].

Differences in homeostatic dynamics also contribute to the great phylogenetic diversity of sleep–wake behavior [17,18,26,27]. This diversity includes distinct sleep patterning (polyphasic or monophasic), timing (nocturnal, diurnal, crepuscular), and sleep need. The physiology of neuronal sleep–wake regulatory networks is largely conserved across mammalian species, but modulation of these networks by homeostatic and circadian inputs can produce a wide range of observed sleep–wake dynamics.

Mathematical modeling has contributed to our understanding of the effects of changing homeostatic dynamics on sleep patterns. Previous modeling studies of sleep—wake regulation examined implications of homeostatic variation for inter-species differences [26] and changes in sleep from adolescence to old age [28]. These results support a key role for homeostatic time constants in producing distinct patterns of sleep—wake behavior. In addition, previous studies have analyzed the types and sequences of bifurcations produced as homeostatic time constants changed [28–30]. However, this previous work focused on models that simulate only two behavioral states, wake and sleep, and do not account for NREM–REM alternation during the sleep episode.

As a first step in understanding the effects of NREM-REM alternation on homeostatically driven changes in sleep patterns, we present a computationally-based analysis of the bifurcations in sleep patterns produced by varying homeostatic time constants in a three-state sleep-wake regulatory network model. This work provides novel insights into the potential role of NREM-REM alternation in the evolution of sleep-wake behavior across development. To analyze the types of bifurcations that occur in the piecewise smooth sleep-wake network model, we construct circle maps that represent key dynamics of the full sleep-wake network model [31]. By computing representative maps for

distinct intervals of homeostatic time constants, we gain insight into the types of bifurcations that occur and elucidate the effects of NREM–REM alternation on sequences of bifurcations in sleep patterns.

The paper is organized as follows: in Section 2 we briefly review the three-state sleep—wake regulatory network model and describe the numerically-constructed one-dimensional circle map that captures the key dynamics of the full model; in Section 3 we describe the bifurcations produced by varying the time constants of the homeostatic sleep drive with a specific focus on the transition between biphasic and monophasic daily sleep patterns; and in Section 4 we provide a brief summary of our results, relate them to previous results in two-state models of sleep—wake regulation, and discuss implications for sleep in early childhood.

### 2. Model and methods

In this section we first describe our three-state sleep—wake regulatory network model and then discuss the methods to construct the circle maps that are used to identify bifurcations of model solutions as homeostatic time constants are varied.

### 2.1. Three-state sleep-wake network model

We utilize our previously developed, sleep-wake regulatory network model to simulate sleep-wake behavior [22,32,33]. This model is based on neurotransmitter-mediated interactions between neuronal populations that promote the states of wake, NREM and REM sleep (Fig. 1). Representative wake-promoting monoaminergic populations include the locus coeruleus (LC) and the dorsal raphe (DR); NREM sleep-promoting populations include GABAergic, sleep-active neurons of the ventrolateral preoptic nucleus (VLPO); and REM-promoting populations include the REM-active, cholinergic areas of the laterodorsal tegmental nucleus (LDT) and pedunculopontine tegmental nucleus (PPT). In the model, mutual inhibition between the wake-promoting and NREM sleep-promoting populations introduces a flip-flop switch governing transitions between sleep and wake states. Transitions between NREM and REM sleep states are dictated according to the reciprocal interaction hypothesis for REM sleep [34], in which the wake-promoting population projects inhibitory synapses to the REM sleep-promoting population, while the REM sleep-promoting population projects excitatory synapses back to the wake-promoting population. The model also represents the suprachiasmatic nucleus (SCN), the hypothalamic region that acts as the central circadian rhythm pacemaker, is entrained to the environmental light cycle, and displays a 24-hour variation in neural firing. SCN projections to sleep/wake regulatory populations drive the 24 h timing of sleep and wake states. For humans under normal light:dark conditions, the circadian rhythm and the sleep-wake cycle are entrained such that sleep occurs when SCN firing rates are low (typically during the dark period), and wake occurs when SCN firing rates are high (typically during the light period). The timing of sleep and wake episodes is additionally influenced by the homeostatic sleep drive. The somnogen adenosine accumulates during periods of wakefulness, decays during sleep, and likely represents a biophysical substrate for the homeostatic sleep drive: high adenosine concentrations increase the activity of VLPO neurons [4,35-38]. We model this effect by letting the activation of the NREM-promoting population depend on the level of the modeled homeostatic sleep drive.

### Neuronal populations

Neuronal population activity is modeled using a firing rate formalism. Instead of tracking the spiking of single neurons, the firing rate model describes the averaged behavior of spike rates of the neuronal populations,  $f_W$ ,  $f_N$ ,  $f_R$ , where W, N, and R denote Wake, NREM and REM, respectively. The neurotransmitter concentration released as a result of activity of the presynaptic neuronal population depends on the mean firing rate of the presynaptic neuronal population. In particular,

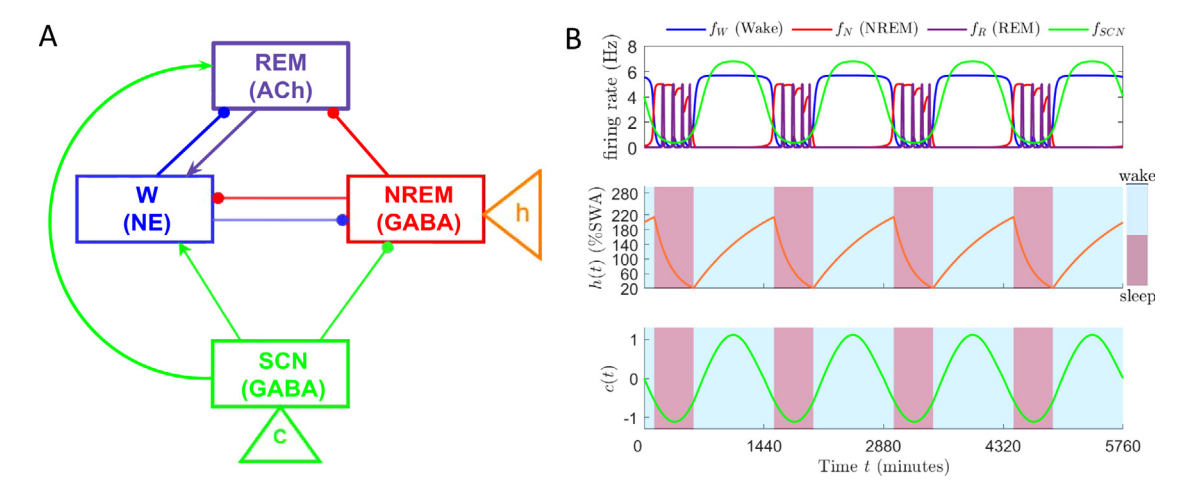


Fig. 1. A physiologically based, three-state model for sleep-wake regulation. A: Schema of the model network summarizing interactions among the wake-promoting, NREM-promoting, REM-promoting and suprachiasmatic nucleus (SCN) neuronal populations with circles denoting inhibitory and arrows denoting excitatory synaptic connections. The representative neurotransmitters for each populat ion are also indicated (NE: noradrenaline, ACh: acetylcholine, GABA: gamma aminobutyric acid). B: Time traces showing the evolution of the model variables corresponding to the stable solution with one daily sleep episode. The top panel includes the firing rates  $f_W$  (Wake),  $f_N$  (NREM),  $f_R$  (REM),  $f_{SCN}$ . The middle panel shows the evolution of the sleep homeostat, h, and the bottom panel shows the evolution of the circadian drive, c. The light blue and rose backgrounds correspond to the times at which the model is in wake and sleep, respectively.

we assume that a firing rate  $f_X$  induces instantaneous expression of neurotransmitter concentration that is described by its steady state function:  $C_i(f_X) = \tanh\left(\frac{f_X}{\gamma_i}\right)$ , where X = W, N, R, SCN and corresponding i = NE (noradrenaline), G (GABA), ACh (acetylcholine), S (GABA expressed by the SCN). The postsynaptic firing rates,  $f_X(t)$  (in Hz), saturate to their steady state firing rate response functions with time constants  $\tau_X$  for X = W, N, R, SCN. The steady state firing rate functions,  $X_\infty(\cdot)$ , have a sigmoidal profile that has been utilized in many firing rate models [26,39–42]. In particular,

$$X_{\infty}(z) = \frac{X_{max}}{2} \left[ 1 + \tanh\left(\frac{z - \beta_X}{\alpha_X}\right) \right] \tag{1}$$

Hence, in this formalism the firing rates  $f_X$  for X = W, N, R, SCN are governed by the following equations:

$$\frac{df_W}{dt} = \frac{W_{\infty} \left(g_{ACh,W} C_{ACh}(f_R) + g_{S,W} C_S(f_{SCN}) - g_{G,W} C_G(f_N)\right) - f_W}{\tau_W}$$
(2)

$$\frac{df_N}{dt} = \frac{N_{\infty}\left(-g_{NE,N}C_{NE}(f_W) - g_{S,N}C_S(f_{SCN}) - g_{G,N}C_G(f_N)\right) - f_N}{\tau_N} \tag{3}$$

$$\frac{df_R}{dt} = \frac{R_{\infty} \left(g_{ACh,R}C_{ACh}(f_R) - g_{NE,R}C_{NE}(f_W) - g_{S,R}C_S(f_{SCN}) - g_{G,R}C_G(f_N)\right) - f_R}{\tau_R} \tag{4}$$

$$\frac{df_{SCN}}{dt} = \frac{SCN_{\infty}(c(t)) - f_{SCN}}{\tau_{SCN}}$$
 (5)

The parameters  $X_{max}$ ,  $\alpha_X$ , and  $\beta_X$  represent the maximum firing rate, sensitivity of response, and half-activation threshold, respectively. Note that  $\beta_X$  is a constant for X=W, R, SCN, whereas  $\beta_N$  is a function that depends on the homeostatic sleep drive described below (see Eq. (7)). The weights  $g_{i,X}$  convert the concentrations  $C_i$  into effective synaptic input. A positive sign in front of  $g_{i,X}$  denotes excitation of the postsynaptic population X due to release of the neurotransmitter i; a negative sign denotes inhibition.

### Circadian drive

The argument of the steady state response function for the SCN firing rate is a fixed circadian drive c(t) as described by a human circadian clock model developed by Forger and colleagues and based on a modified van der Pol oscillator [43,44]. The circadian drive c(t) represents the phase of core body temperature and is influenced by light intensity, which is an explicit input to the model. Here, we assume the circadian oscillator is entrained to a 24 h environmental light schedule which is simulated by a 14:10 Light:Dark cycle with a light input of 500 lux during the light period and 0 lux during the dark period. A time trace of the circadian drive c(t) is shown in Fig. 1B (bottom panel). For a more detailed description of this model, see Appendix A.

### Homeostatic sleep drive

The modeled homeostatic sleep drive (h) regulates sleep propensity, and its dynamics are based on experimentally observed variation in the power of slow wave (0.75–4.5 Hz) activity in electroencephalogram (EEG) recordings during sleep. The levels of the homeostatic drive increase exponentially with the time constant  $\tau_{hw}$  during wake and decrease exponentially with the time constant  $\tau_{hs}$  during sleep according

$$\frac{dh}{dt} = \frac{\mathcal{H}(f_W - \theta_W) \cdot (h_{max} - h)}{\chi \tau_{hw}} + \frac{\mathcal{H}(\theta_W - f_W) \cdot (h_{min} - h)}{\chi \tau_{hs}}$$
(6)

where  $\mathcal H$  represents a Heaviside function,  $\theta_W$  is the threshold demarcating states of wake and sleep, and h is in units of percent Slow Wave Activity (SWA) power. The parameter  $\chi$  is used to scale the time constants in our bifurcation analysis. The values of the time constants  $\tau_{hw}$  and  $\tau_{hs}$ , namely when  $\chi=1$ , are set to experimentally determined values for typical adult human sleep behavior [13].

It is important to note that h is a piecewise smooth variable which makes the model system piecewise smooth. As discussed below, this affects the methods available to analyze model solutions.

The mechanism of action of the sleep drive h is based on adenosine [4,35–38] and is implemented as modulation of the activity of the NREM-promoting population through  $\beta_N(h)$  as follows:

$$\beta_N(h) = k_2 \cdot h + k_1. \tag{7}$$

The parameters  $k_1$  and  $k_2$  are measured in effective synaptic input and effective synaptic input/(% mean SWA), respectively, and together determine the contribution of h to the response of the NREM-promoting population. Thus, as h increases during wake, the sleep promoting population will eventually activate to inhibit the wake population and

Table 1

Default parameter values for the network model for human monophasic sleep. For X=W,N,R,SCN,  $\alpha_X$  and  $\beta_X$  are in units of effective synaptic input.  $\beta_N$  is not included here because it is a function (Eq. (7)). Additionally, for  $i=NE,G,ACh,S,g_{iX}$  has units of (effective synaptic input/Hz). Units for  $h_{max}$  and  $h_{min}$  are percentage mean SWA. The parameters  $k_1$  and  $k_2$  are measured in effective synaptic input and effective synaptic input/(% mean SWA), respectively. The remaining units are included in the table.

Firing rate parameters (Eqs. (1)–(5))			
$W_{max} = 6 \text{ Hz}$	$\tau_W = 23 \text{ min}$	$\alpha_W = 0.4$	$\beta_W = -0.4$
$N_{max} = 5 \text{ Hz}$	$\tau_N = 10 \text{ min}$	$\alpha_N = 0.2$	
$R_{max} = 5 \text{ Hz}$	$\tau_R = 1 \text{ min}$	$\alpha_R = 0.1$	$\beta_R = -0.8$
$SCN_{max} = 7 \text{ Hz}$	$\tau_{SCN} = 0.5 \text{ min}$	$\alpha_{SCN} = 0.7$	$\beta_{SCN} = -0.1$
Synaptic weights (Eqs. (2)–(4))			
$g_{ACh,W} = 0.8$	$g_{S,W} = 0.1911$	$g_{G,W} = 1.4928$	
$g_{NE,N} = 1.5$	$g_{S,N} = 0.2141$	$g_{G,N} = 0$	
$g_{ACh,R} = 2.2$	$g_{NE,R} = 10.7473$	$g_{S,R} = 0.8$	$g_{G,R} = 1.07$
Homeostatic parameters (Eqs. (6), (7))			
$h_{max} = 323.88$	$h_{min} = 0$	$\tau_{hw} = 946.8 \text{ min}$	$\tau_{hs} = 202.2 \text{ min}$
$k_1 = -0.1$	$k_2 = -0.0045$	$\theta_W = 2 \text{ Hz}$	$\chi = 1$

cause the model to transition to sleep. Conversely, as h decreases during sleep, the sleep population will eventually inactivate and allow the wake population to activate. We define sleep onset to occur when  $f_W$  decreases below  $\theta_W$  (and h starts to decrease) and wake onset to occur when  $f_W$  increases above  $\theta_W$  (and h starts to increase).

Default monophasic sleep-wake behavior in the three-state model

All default model parameter values are given in Table 1. For these parameter values, the model produces a stable solution representing a monophasic sleep pattern consistent with sleep—wake behavior in adult humans. In particular, this solution is characterized by 16.11 h of wake and 7.89 h of sleep including 6.58 and 1.31 h of NREM and REM sleep, respectively (Fig. 1). During each sleep episode, alternation between NREM and REM sleep produces four distinct REM bouts. The sleep onset circadian phase,  $\Phi$ , is defined as the time difference between sleep onset ( $t_{so}$ ) and the preceding minimum of the circadian drive variable c ( $t_{cmin}$ ), divided by the period of the circadian oscillator entrained to the light/dark cycle (24 h). That is:

$$\Phi = \frac{t_{so} - t_{cmin}}{24}.\tag{8}$$

Thus, we have  $f_W(t_{so})=\theta_W$ . In addition, if D is a 24 h interval such that  $t_{cmin}\in D$ , then we have  $c(t_{cmin})=\min_{t\in D}\{c(t)\}$  and  $0\leq t_{so}-t_{cmin}<24$ . For example,  $\Phi=0$  corresponds to the sleep onset occurring at the minimum c(t) value, and  $\Phi=0.5$  corresponds to the sleep onset occurring at the maximum c(t) value. For the stable default solution,  $\Phi=0.829$ , so the sleep onset occurs on the decreasing phase of c. This is consistent with the relationship between sleep onset and the phase of core body temperature in typical adult human monophasic sleep behavior.

In the following section, we describe the techniques used to analyze the dynamics of our three-state model. Note that in previous work involving a two-state model of sleep—wake regulation we proposed the same mathematical framework [29]. We provide a detailed discussion of this framework and highlight similarities and differences in the dynamics of the two- and three-state models.

### 2.2. One-dimensional circle map

To analyze model solutions and their bifurcations, we construct circle maps that describe the relationship between the circadian phases of successive sleep onsets [29,31,45]. As described above, we define sleep onset to be the time at which  $f_W$  decreases through the threshold  $\theta_W$ . To construct the map, we numerically integrate the model forward in time from initial conditions with  $f_W = \theta_W$  across the full range of circadian phases (dictated by values of c) and track the circadian

phases at which the trajectories next cross the  $f_W=\theta_W$  section. To set such initial conditions, we need to determine appropriate values for the other model variables, namely  $f_N$ ,  $f_R$ ,  $f_{SCN}$ , h as well as the additional variables for the circadian clock model, that satisfy model equations on the  $f_W=\theta_W$  section at different circadian phases. To do that, we consider a fast–slow decomposition of the model to identify variable values at sleep–wake transitions, as described in Section 2.2.1. In Section 2.2.2, we describe the details of map computation and show the map for the default parameter set (Table 1).

### 2.2.1. Fast-slow decomposition

To understand model dynamics, we consider a fast–slow decomposition of the model system. The decomposition exploits the slow time scales of the circadian oscillator and homeostatic sleep drive compared to the faster firing rates of the neuronal populations. As in [31], we consider the fast subsystem to consist of the firing rates of all neuronal populations by defining  $\mathbf{F}(t) = \{f_W(t), f_N(t), f_R(t), f_{SCN}(t)\}$ . The slow subsystem then consists of the circadian and homeostatic sleep drives defined by  $\mathbf{S}(t) = \{h(t), \mathbf{c}(t)\}$  where  $\mathbf{c}(t)$  consists of the three variables for the circadian clock model, including c(t) (see Appendix A). In particular, the full model system can be written as follows:

$$\frac{d\mathbf{F}}{dt} = \mathbf{M}(\mathbf{F}, \mathbf{S}) \tag{9}$$

$$\frac{d\mathbf{S}}{dt} = \epsilon \mathbf{N}(\mathbf{F}, \mathbf{S}) \tag{10}$$

where M consists of Eqs. (2)–(5) and N consists of Eq. (6) and Eqs. (A.1)–(A.3). We assume  $0 < \epsilon \ll 1$ . Coupling of the fast and slow subsystems occurs due to the dependence of  $f_N(t)$  on h(t) in Eq. (7), and of  $f_{SCN}(t)$  on c(t) in Eq. (5).

In the limit  $\epsilon \rightarrow 0$  when h and c are constants, we compute the steady state solutions of the fast subsystem, M(F,S) = 0, with respect to the bifurcation parameter h for different values of c (using XPP/XPPAUT [46]). The resulting bifurcation diagram, when represented in terms of the firing rate  $f_{W}$  of the wake-promoting population, forms a Z-shaped curve with respect to h at each value of c(Fig. 2A). The upper branch of the Z-shaped curve comprises stable steady state solutions corresponding to the wake state. The middle and lower branches correspond to unstable fixed points of the fast subsystem, and the folds of the Z are saddle-node bifurcation points where two steady states coalesce. Associated with the lower branch of unstable solutions are stable periodic solutions corresponding to NREM-REM alternation or cycling in which the REM firing rate  $f_R$ displays high amplitude oscillations and  $f_W$  displays low amplitude oscillations. The unstable fixed points of the fast subsystem separate the basins of attraction for the stable fixed point and the stable periodic solution. For each fixed c value, we obtain similar solutions with respect to h which collectively form a Z-shaped fast-slow surface on which trajectories of the full system ( $\epsilon > 0$ ) evolve (Fig. 2B).

Solution trajectories of the full model traverse the lower manifold of this surface during the sleep state with the periodic solutions corresponding to NREM–REM cycling which occurs at different frequencies depending on the strength of the circadian drive c (Fig. 2C). Lower values of c lead to lower frequency NREM–REM cycling with longer REM bouts, while higher values of c yield higher frequency cycling with shorter REM bouts. Additionally, NREM–REM cycling is more sensitive to changes in the strength of the circadian drive than in the strength of the homeostatic sleep drive.

In the full model, transitions between sleep and wake states occur when solution trajectories traverse over the curves of saddle–node points forming the folds of the Z-surface. Sleep onset is initiated when solution trajectories cross over the upper saddle–node curve and is defined when the trajectory decreases through the  $f_W = \theta_W$  section. Wake onset occurs when trajectories pass near the lower saddle–node curve and increase to the upper manifold of the Z-surface. Thus, by considering the fast–slow decomposition, we obtain steady state values of all model variables near the transition from wake to sleep.

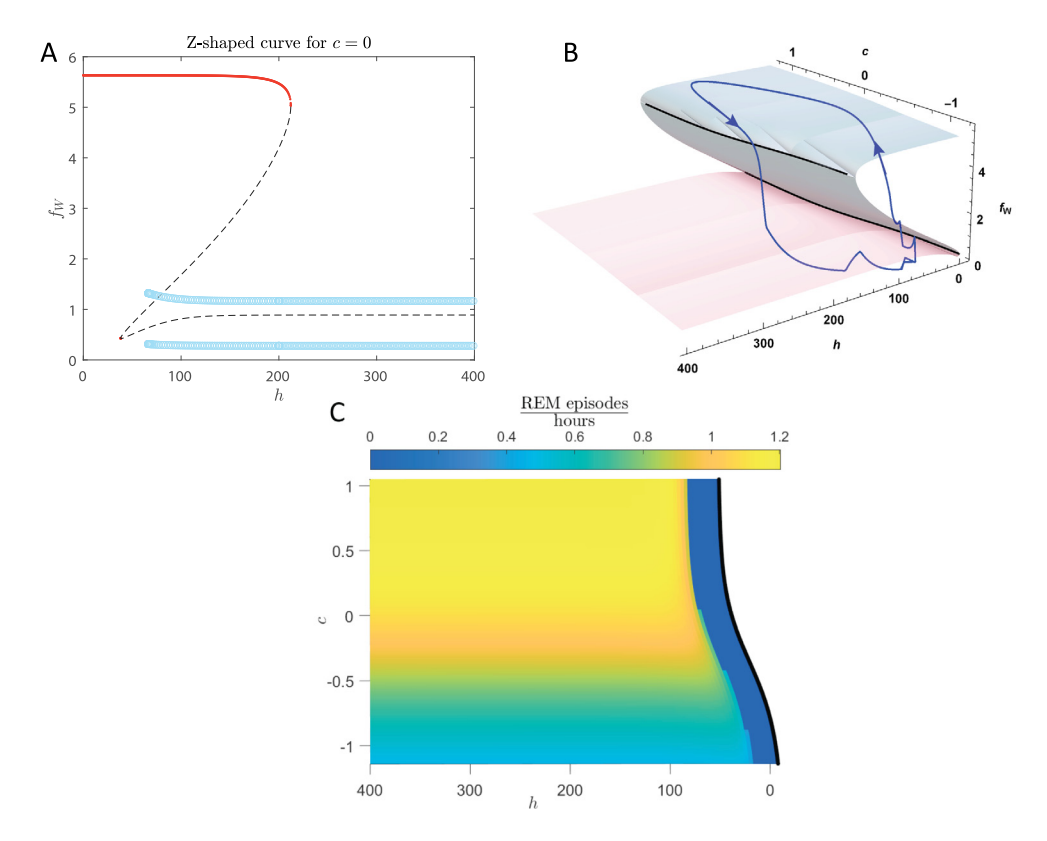


Fig. 2. Fast–slow decomposition of the three-state sleep–wake model. A. The Z-shaped curve obtained by the fast–slow decomposition for c=0 illustrates the steady state solutions of the variable  $f_W$  as a function of the varying parameter, h. The red solid and black dashed curves correspond to stable and unstable steady state solutions of the fast subsystem, respectively. The light blue circles correspond to the periodic solution representing the NREM–REM cycling occurring during the sleep state. B. The fast–slow Z-shaped surface for varying h and c values and the stable orbit (blue curve) of the model for the default parameter set. C. Frequency plot of NREM–REM cycling for various values of the parameters c and h, corresponding to the periodic solutions in the fast subsystem during the sleep state. The black curve corresponds to the lower saddle–node points of the Z-shaped surface. The darkest blue region (to the left of the saddle–node curve) corresponds to (h,c) values for which the stable solution of the fast subsystem is not periodic and corresponds to the wake state.

In previous work, we have shown that a two-state sleep—wake network model has a similar Z-shaped bifurcation diagram for each fixed value of the circadian drive and varying homeostatic sleep drive [29,47]. In that case, the lower branch of the Z-shaped curve is stable, and the mechanism for transition from sleep to wake is the passage through the lower saddle—node curve. In contrast, transitions from sleep to wake in the three-state model are influenced by the interaction of the lower saddle—node curve with the periodic solutions representing NREM—REM cycling [47].

### 2.2.2. Constructing the circle map

As described above, to construct the circle map we need to specify initial conditions for all model variables corresponding to solutions on the section  $f_W = \theta_W$  at each circadian phase. From the fastslow decomposition, we know that trajectories decreasing through the  $f_W = \theta_W$  section would have previously passed across the upper curve of saddle–node points of the Z-surface. Thus, to obtain the appropriate initial conditions, we numerically integrate the full model from values on or near the upper saddle-node curve of the Z-surface and set the initial conditions for the map to the solution at the first crossing of the  $f_W = \theta_W$  section. Specifically, to initiate the model integration, the values of the neuronal population firing rates,  $f_W, f_N, f_R$  and the homeostatic sleep drive, h, are set to values on or near the upper saddle–node curve at a fixed value of c, and the circadian clock-related variables, namely the SCN firing rate  $f_{SCN}$  and the other clock model variables, are set to values determined by the stable solution of the circadian clock model associated with the same fixed value of c. The values of the upper saddle-node curve were computed using twoparameter numerical continuation of the saddle-node bifurcation in the h-c plane (implemented in AUTO on XPPAUT [46] with adaptive step size in c). From these points, model trajectories typically immediately decreased through the  $f_W = \theta_W$  section. To obtain a full set of initial conditions for the map, we considered c over one circadian cycle (approximately -1.115 < c < 1.115). To construct the map,  $\Pi$ , we plot the circadian phase of the (n+1)st sleep onset,  $\Phi_{n+1} = \Phi(t_{so}^{n+1})$ , as a function of the nth sleep onset circadian phase,  $\Phi_n = \Phi(t_{so}^n)$ , both obtained by numerical integration of the full model. Thus,

$$\Pi: \Phi_n \mapsto \Phi_{n+1}. \tag{11}$$

Assumption of a fixed light:dark schedule is required for the map computation to maintain a rigorous definition of circadian phase, but, based on previous work, we expect that similar results would be obtained if light intensity was allowed to vary with behavioral state (see [45] and Discussion for more details). All map computations were performed in MATLAB (MathWorks Inc., Natick, MA). More details regarding the construction of the map can be found in [31].

### 2.2.3. Features of the circle map

The map for the three-state sleep-wake model is piecewise smooth and non-monotonic. The non-monotonic nature of individual map branches renders it noninvertible. Furthermore, it exhibits both large vertical discontinuities or gaps, and smaller gaps occurring at cusps that separate distinct branches of the map (Fig. 3). The separate branches of the map correspond to sleep-wake cycles with distinct sleep and wake bout durations, and numbers of REM bouts. Note that the number of REM bouts associated with each branch of the circle map is determined separately by simulating the model from the same initial conditions used to derive the map. For default parameter values, the map has one stable fixed point at  $\Phi_n=0.829$  corresponding to the stable periodic solution displayed in Fig. 1. This solution has one sleep

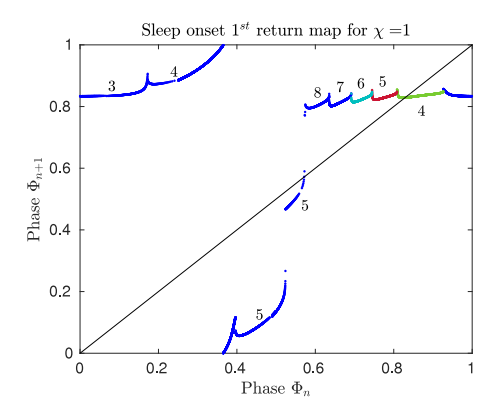


Fig. 3. One dimensional circle map illustrating the circadian phase of the n+1st sleep onset,  $\boldsymbol{\Phi}_{n+1}$  as a function of circadian phase of the nth sleep onset,  $\boldsymbol{\Phi}_n$ . For each branch of the map we indicate the distinct number of REM bouts occurring in sleep episodes initiated at the associated circadian phase. We distinguish the branches representing 4 REM bouts (green), 5 REM bouts (red) and 6 REM bouts (light blue), as these are significant for our later analysis. Note that the number of REM bouts associated with each branch of the circle map is determined separately.

episode per circadian day with a duration of 7.89 h; each sleep episode contains four REM bouts. Using the cobwebbing method on the map (see e.g. [48] for an explanation of the method), we can track the reentrainment process from initial phases of sleep onsets distinct from the fixed point back to the stable periodic behavior.

The map exhibits a large vertical gap close to the phase associated with the peak of the circadian drive ( $\Phi_n = 0.5$ ). The left branch at the discontinuity has an infinite slope which is a consequence of trajectories starting from these initial conditions approaching a tangent intersection with the saddle-node curves of the Z-shaped surface, referred to as a grazing bifurcation [49]. In particular, trajectories on either side of the gap represent sleep onsets at similar phases (when the circadian drive is very close to its peak), and these trajectories evolve close to each other through the sleep episode and transition to wake at similar phases. However, the trajectory initiated on the infinite slope of the map branch at the left of the gap exhibits a short wake episode as it jumps down from the upper saddle-node curve and transitions to sleep, thereby resulting in the next sleep onset phase of about  $\Phi_{n+1} = 0.1773$ . By contrast, the trajectory initiated on the map branch at the right of the gap approaches the upper saddle-node curve tangentially, resulting in a longer wake episode. As this trajectory evolves further, the subsequent sleep onset occurs at a phase of about  $\Phi_{n+1} = 0.4667$ .

Similar grazing bifurcations characterize discontinuities in maps constructed from two-state sleep—wake models [29,30]. In a two-state model similar to the three-state model presented here, transitions to sleep and wake occur by passage through saddle—node curves and opportunities for trajectories to evolve tangentially to these curves occur at both state transitions [29]. We note that for the simpler Two-Process model, the upper and lower circadian threshold curves play a similar role to the saddle—node curves in our higher-dimensional models [30].

However, maps of the three-state model are characterized by additional discontinuities. Indeed, the unique features of maps for the three-state model are the cusp gaps between map branches for trajectories with distinct numbers of REM bouts. The number of REM bouts during a sleep episode depends on how the trajectory traverses the periodic solutions on the lower manifold of the *Z*-surface, especially as it approaches the lower curve of saddle nodes. These periodic solutions exist due to the reciprocal interactions between the REM-and wake- promoting populations of the three-state model. Trajectories that are initiated at similar sleep onset phases may approach the lower saddle–node curve at slightly different circadian phases resulting in a difference of one REM bout and thus different subsequent sleep

onset phases, placing their corresponding phase points on distinct map branches. As we illustrate below, these cusp gaps significantly affect the model's stable orbits as homeostatic time constants are varied, introducing additional bifurcations that are not observed in two-state sleep–wake network models.

### 2.3. Varying the dynamics of the homeostatic sleep drive: our framework

In this work, we investigate the effects of NREM–REM alternation on bifurcations occurring in the transition between polyphasic (multiple sleeps per day) and monophasic (one sleep per day) sleep behavior. For our analysis purposes, we start with default parameters generating monophasic sleep and induce polyphasic sleep by decreasing the time constants of the homeostatic sleep drive h. We scale the time constants  $\tau_{hw}$  and  $\tau_{hs}$  by the parameter  $0 < \chi \le 1$  (see Eq. (6)). Thus, as  $\chi$  decreases, h grows and decays more quickly causing sleep propensity to accumulate and dissipate faster, respectively.

We will use the following notation to indicate the numbers of sleep episodes per circadian cycle and REM bouts per sleep episode in stable solutions. A stable sleep pattern that repeats after n circadian cycles is represented as

$$\{p_{r1}^1, p_{r2}^2, \dots, p_{rn}^n\}^{\infty},$$
 (12)

where the number  $p^i$  gives the number of sleep episodes on the ith circadian cycle and ri is a  $p^i$ -tuple whose entries represent the number of REM bouts in each sleep episode represented in  $p^i$ . For example, the default solution at  $\chi=1$ , consisting of one sleep episode with 4 REM bouts in each circadian cycle, is represented as  $\{1_4\}^\infty$ . At  $\chi=0.8625$ , a stable 2-cycle in which two distinct sleep episodes with 4 REM bouts occurring on alternating circadian cycles is represented as  $\{1_4,1_4\}^\infty$ . At  $\chi=0.649$ , a pattern that alternates between 1 and 2 sleeps per circadian cycle is represented as  $\{1_3,2_{(4,3)}\}^\infty$ . On the first circadian cycle one sleep episode involving 3 REM bouts  $(1_3)$  occurs. On the second circadian cycle, two sleep episodes occur: one involves 4 REM bouts, and the other involves 3 REM bouts  $(2_{(4,3)})$ .

To quantify the sleep episode patterns generated as  $\chi$  is decreased, we define a 'rotation number' of sleep episodes,

$$\rho = \frac{q}{p} \,, \tag{13}$$

where p is the number of sleep episodes in the pattern occurring over q circadian days [50]. If a stable pattern is not detected, we approximate  $\rho$  to be the average number of the total circadian days divided by the total sleep episodes in a 120 day simulation.

Similarly, to quantify NREM–REM alternation or cycling patterns during sleep episodes, we define a 'REM rotation number' as  $\tilde{\rho}_{REM} = \frac{p}{r}$ , where r is the number of REM bouts occurring during the p sleeps in the pattern. If a stable pattern cannot be detected, we approximate  $\tilde{\rho}_{REM}$  by the total number of sleep episodes divided by the total number of REM bouts in a 120 day simulation.  $\tilde{\rho}_{REM}$  takes on values less than 1 in physiologically-relevant parameter regimes. However, since it is more intuitive to talk about REM episodes per sleep, we will use the reciprocal of the REM-rotation number for the rest of this study. We will denote that as  $\rho_{REM}$  and refer to it as the 'REM rotation number' for simplicity. Thus,

$$\rho_{REM} = \frac{r}{p} \,. \tag{14}$$

Based on these definitions,  $\rho=1$  and  $\rho_{REM}=4$  for both of the distinct stable sleep patterns for  $\chi=1$  and  $\chi=0.8625$  discussed above. The sleep pattern for  $\chi=0.649$  is associated with  $\rho=\frac{1}{2}$  and  $\rho_{REM}=\frac{10}{3}$ .

In the analysis below, we investigate whether there is an underlying structure in  $\rho$  and  $\rho_{REM}$  as  $\chi$  is reduced.

For example, one such structure in the rotation number emerges from a period-adding cascade triggered by a border collision bifurcation, as occurs in two-state sleep-wake models [28–30]. A border

collision in the kth return map occurs when the border at a discontinuity of the map curve intersects the diagonal,  $\Phi_{n+k} = \Phi_n$ , and results in the creation or destruction of a fixed point (stable or unstable). This border collision bifurcation in the map corresponds to a grazing bifurcation when an orbit (stable or unstable) makes a tangent intersection with the saddle–node curves of the Z-shaped surface (Fig. 2B).

A resulting period-adding bifurcation sequence dictates that the average number of sleep episodes per circadian cycle, i.e. the reciprocal of the rotation number as defined above, follows a predictable sequence that can be characterized by a Farey sequence. Elements of the Farey sequence obey the Farey addition. Namely, in between neighboring intervals of the varying parameter displaying solutions with rotation numbers  $\rho_1 = \frac{q}{p}$  and  $\rho_2 = \frac{q'}{p'}$ , where  $\gcd(q,p) = 1$ ,  $\gcd(q',p') = 1$  and |qp'-pq'|=1, there exists an interval of the parameter with rotation number  $\rho = \frac{q+q'}{p+p'}$ . For example, in a period adding bifurcation, in the parameter intervals between those producing stable monophasic and biphasic sleep patterns, one finds stable patterns involving combinations of circadian cycles with 1 or 2 sleep episodes per cycle such that there are more cycles with 1 sleep per day as the parameter approaches the monophasic sleep regime and more cycles with 2 sleeps per day as the parameter approaches the biphasic sleep regime.

When a period-adding bifurcation sequence occurs, the rotation number is a Cantor function or a Devil's staircase in terms of the varying parameter (namely a monotonic, continuous function that has derivative equal to 0 almost everywhere that attains every rational number in the Farey sequence).

### 2.4. Motivation from results in two-state models of sleep-wake regulation

In two-state sleep-wake models including the Two Process model and simple sinusoidal threshold systems under similar parameter variations, numerical simulations have detected this underlying Devil's staircase-like structure in  $\rho$  as homeostatic time constants or other parameters are varied [29,30]. These findings suggest that although higher-order patterns of napping/non-napping behavior may occur during this transition, unique behavior is associated with each parameter combination and the progression to consolidated sleep is monotonic. In [29] we employed similarly constructed circle maps and identified sequences of border collision and saddle-node bifurcations leading to the loss or birth of stable solutions. We also showed that the transition between polyphasic and monophasic sleep can be influenced by features of the SCN firing rate (Eq. (5)), such as its steepness and peak activity duration. In particular, longer duration of the peak activity of the SCN firing rate promotes the existence of the biphasic and monophasic pattern, but fewer intermediate patterns. Therefore, interactions between the homeostatic and circadian components can lead to an easier or more challenging transition from napping to nonnapping behavior. Here, we investigate how NREM-REM alternation or cycling may affect sleep patterning under developmentally-mediated changes in homeostatic dynamics. In particular, we focus on identifying features characterizing the transition from napping to non-napping behavior that two-state models fail to capture.

### 3. Results

In the three-state sleep—wake model representing wake and NREM-REM alternation, we find complex sequences in the transitions of solutions as the homeostatic sleep drive time constants are decreased. In contrast, previous work in two-state sleep—wake models showed that similar changes in homeostatic dynamics produced well-structured, period-adding bifurcation sequences during the transition between polyphasic and monophasic sleep [28–30].

In the three-state model, while the Farey sequence in sleep episodes per circadian cycle is overall generally retained, bifurcations in NREM—

REM cycling disrupt the period-adding structure and introduce additional features including apparent period-doubling cascades and intervals of bistability. More complex bifurcation sequences can be expected in the three-state model since the circle maps are non-invertible which can lead to non-uniqueness of solutions [51] and, thus, of the rotation number of either sleep or REM episodes. However, the additional complexity associated with the occurrence of NREM–REM cycling in the three-state model suggests that sleep architecture interacts with developmentally-mediated changes in sleep and may contribute to toddler sleep variations [52], and potential problems [53].

For default homeostatic time constants, when the scaling parameter  $\chi = 1$ , the model produces a stable solution corresponding to the typical adult sleep pattern of one consolidated nocturnal sleep episode per day. As  $\gamma$  is decreased, we find  $\gamma$  intervals that generate polyphasic sleep solutions consisting of regular daily sleep patterns involving more than one sleep episode per day. For example, an average of two sleep episodes per day occurred for  $\chi \in [0.41, 0.542]$ , and three sleep episodes per day occurred for  $\chi \in [0.264, 0.29]$  (Fig. 4). Between the  $\chi$ -intervals associated with fixed n and n + 1 sleep episodes per day, there are  $\chi$  values associated with higher order sleep patterns that occur over several circadian days and involve some days with n sleeps and some days with n + 1 sleeps. For example,  $\chi = 0.65$  falls between  $\chi = 1$ (with one sleep per day) and  $\chi = 0.542$  (with two sleeps per day) and is associated with a pattern that alternates between one and two sleeps per day. This pattern would correspond to a child napping every other day.

As described in the Methods, these sleep patterns may be quantified with a 'rotation number' of sleep episodes,  $\rho$  (see Eq. (13)). The bifurcation diagram of  $\rho$  as a function of the scaling parameter  $\chi$  (Fig. 4B) depicts stable solutions (black points) and approximate solutions (gray points) obtained after simulating the model for 120 days. In contrast to the two-state models that produce a strict Farey sequence of rotation numbers, we numerically detect rotation numbers that form a subset of the full Farey sequence in the three-state model.

Furthermore, in contrast to the two-state model, rotation numbers in the three-state model do not decrease monotonically with  $\chi$  and are not unique. For example, within the  $\rho=\frac{2}{3}$  interval there are  $\chi$  values that generate a  $\rho=\frac{7}{10}$  stable solution indicating bistability of solutions. Lack of monotonicity in rotation number implies that napping frequency may not decrease monotonically with decreasing homeostatic sleep need.

Additionally, in the three-state model, NREM–REM cycling varies with  $\chi$ . As described in the Methods, we quantify NREM–REM cycling patterns during sleep episodes using a 'REM rotation number'  $\rho_{REM}$  (see Eq. (14)). Stable patterns of NREM–REM cycling are indicated in blue in Fig. 4C. If a stable pattern is not detected, an approximate  $\rho_{REM}$  is computed (gray points).

As  $\chi$  decreases below 1,  $\rho_{REM}$  changes even across  $\chi$  intervals of constant  $\rho$  indicating that the number of REM bouts during sleep episodes changed while the number of sleep episodes per circadian cycle did not. Additionally, bistability is exhibited in the bifurcation diagram of  $\rho_{REM}$ , as there are  $\chi-$  values in which two stable REM rotation numbers were found (Fig. 5).

In the following subsections we describe representative examples of these phenomena focusing on features of the variation in  $\rho$  and  $\rho_{REM}$  as  $\chi$  is decreased and identifying the underlying bifurcations of solutions. We particularly consider the monophasic sleep regime, the transition from monophasic to biphasic sleep, the biphasic sleep regime, and the polyphasic sleep limit.

### 3.1. Bifurcations associated with NREM-REM cycling during monophasic sleep

In this section we focus on the  $\chi$  interval associated with monophasic sleep where  $\rho=1$  ( $\chi\in[0.7235,1]$ ). Changes in NREM–REM cycling are particularly notable over this interval with  $\rho_{REM}$  increasing from

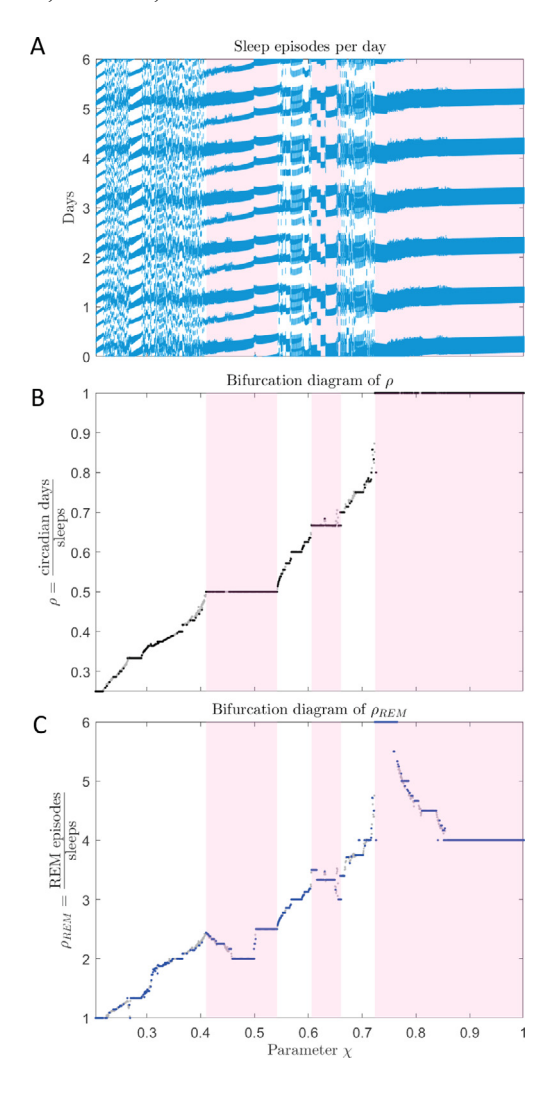
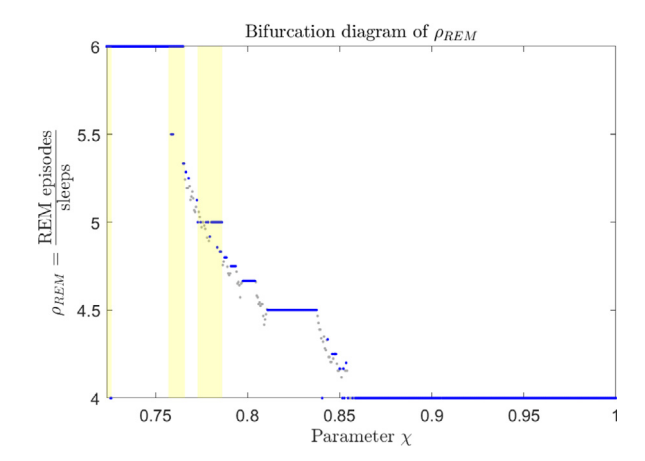


Fig. 4. Summary of sleep patterns and bifurcation diagrams of  $\rho$  and  $\rho_{REM}$  as the homeostatic sleep drive time constants are decreased with respect to the scaling parameter  $\chi$ . The pink shaded regions correspond to  $\chi$ -intervals of  $\rho=1,2/3,1/2$  solutions. A. Patterning of sleep—wake behavior varies with scaling parameter  $\chi$ . Sleep episodes over 6 days (y-axis) are shown as a function of  $\chi$  (x-axis). As  $\chi$  decreases, sleep patterns transition from one sleep episode per day near  $\chi=1$  to two sleep episodes per day near  $\chi=0.29$ . B. Bifurcation diagram of the rotation number,  $\rho$ , denoting stable (black dots) and quasi-periodic (gray dots) solutions with respect to  $\chi$ . The parameter  $\chi$  is on the x-axis and the rotation number  $\rho$ , defined as the number of circadian days over the number of sleep episodes in the stable sleep pattern is on the y-axis. C. Bifurcation diagram of the REM rotation number,  $\rho_{REM}$ , denoting stable (blue dots) and quasi-periodic (gray dots) solutions with respect to  $\chi$ . The REM rotation number,  $\rho_{REM}$ , is defined as the number of REM bouts over the number of sleep episodes in the sleep pattern. For all panels, the step size for  $\chi$  was 0.0005.

4 to 6 (Fig. 5). This reflects potential changes in ultradian cycling during sleep after sleep has been consolidated to a single nocturnal sleep episode but before an individual demonstrates the specific timing, duration, and number of REM bouts characteristic of a typical adult sleep pattern. In addition, we show that  $\rho_{REM}$  values of stable solutions (in blue) in neighboring  $\chi$  intervals are related by Farey addition with apparent period-doubling cascades in intervals of constant  $\rho_{REM}$  and bistability of  $\rho_{REM}$  between some  $\chi$  intervals. To understand the bifurcations that generate the changes in NREM-REM alternation as well as the occurrence of bistability, we employ our sleep onset circle maps. The types of bifurcations observed include saddle-node, period-doubling and border collision bifurcations.



**Fig. 5.** The bifurcation diagram of  $\rho_{REM}$  in the range of  $\chi$  for which  $\rho=1$ . There is an underlying, but not strict, period-adding structure in the sequence of  $\rho_{REM}$  values as  $\chi$  is decreased. In addition, there are intervals of  $\chi$  in which bistability occurs (denoted by the yellow shaded regions).

We explain the bifurcations in the maps and the evolution of sleep patterns as  $\chi$  decreases from 1, and we follow the bifurcation diagram of  $\rho_{REM}$  (Fig. 5) from  $\rho_{REM}=4$  to  $\rho_{REM}=6$ .

 $\rho_{REM}=4$ 

As described above, for the default value  $\chi = 1$ , the sleep onset map exhibits a stable fixed point on the map branch corresponding to 4 REM bouts per sleep episode (green branch in Fig. 3). As  $\chi$  decreases, the map evolves, and the location and stability of the fixed point changes (Fig. 6). For  $1 > \chi > 0.87$ , the fixed point persists on the same map branch and occurs at a slightly earlier circadian phase corresponding to a regular schedule with an earlier habitual bedtime than the default sleep pattern ( $\chi = 1$ ). As  $\chi$  continues to decrease, the fixed point persists; however, at  $\chi = 0.867$  the slope of the map curve at the fixed point has decreased below -1 (Fig. 6A), indicating a loss of stability of the fixed point. For  $\chi$  values in this regime, stable solutions correspond to higher order cycles, and there is no longer a habitual sleep schedule that repeats daily. For example, for  $\chi = 0.8625$  we observe a two day pattern in which one sleep episode occurs on each day, but the sleep onset phases of these sleep episodes are distinct. Both sleep episodes in the pattern contain four REM bouts, however, the REM bouts in each sleep episode occur at distinct circadian phases. This pattern consists of two sleep episodes per two days with 4 REM bouts per sleep episode which yields rotation numbers  $\rho = \frac{2}{3} = 1$  and  $\rho_{REM} = \frac{8}{3} = 4$ . Thus, the loss of stability of the fixed point leads to a period-doubling bifurcation. In this regime, the period of the pattern described by higher order cycles is a power of 2, and all sleep episodes in the pattern contain four REM bouts. These higher order cycles can be illustrated on the map through the method of cobwebbing [48]. In particular, one can determine which map branches are visited and the order in which they are visited by cobwebbing from one of the phases in the stable pattern. For example, for  $\chi = 0.8625$  a cobwebbing cycle of order two exists that alternates between two values on the four-REM-branch on either side of the unstable fixed point (Fig. 6B, two-cycle shown in black). We also include the stable cycle produced by simulating the full model (Fig. 6B, two-cycle shown in purple). The two cycles are close, but exhibit slight differences in phase values, and therefore, a difference of about 8 min in sleep onset times. Such differences are expected, as model variables may have slightly different values under model simulations compared to the ones obtained from map initial conditions. In the remaining maps, we only include the cycles obtained from model simulations, as the phasepoints lie very close to the map curves.

As  $\chi$  decreases slightly further, we find a  $\{1_4, 1_4, 1_4, 1_4\}^{\infty}$  pattern (see expression (12) for an explanation of the notation describing the

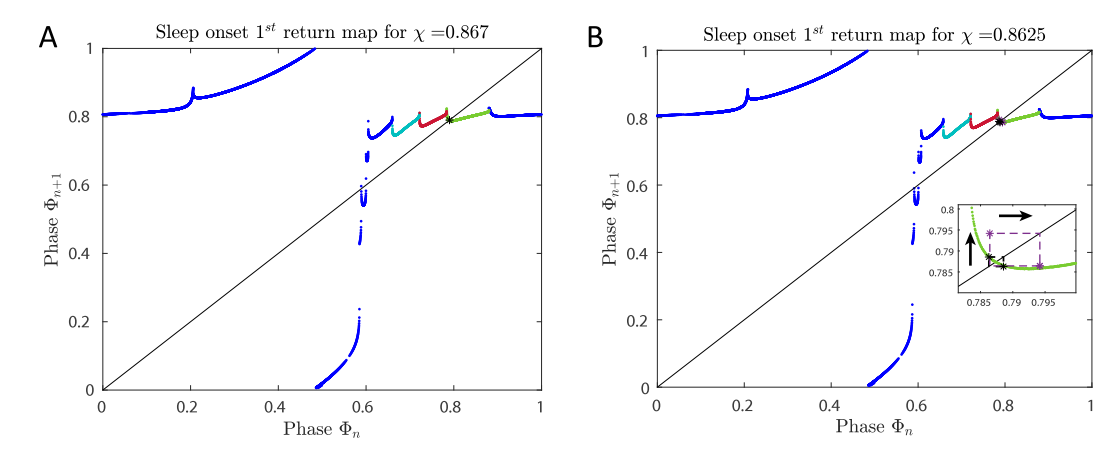


Fig. 6. Maps in the  $\rho=1$ ,  $\rho_{REM}=4$  regime showing a period doubling bifurcation. The green, red and light blue map branches correspond to circadian phases of sleep episodes involving 4, 5, and 6 REM bouts, respectively. A. The first return map for  $\chi=0.867$  has one stable fixed point on the green branch involving sleep episodes with 4 REM bouts. The slope of the map at the fixed point is -1 designating the loss of stability of the fixed point at a period doubling bifurcation. B. The first return map for  $\chi=0.8625$  has one unstable fixed point and a higher (second) order cycle detected by cobwebbing (cycle shown in black in the inset) involving two phase points on the green branch representing sleep episodes with 4 REM bouts. The black arrows in the inset show the direction of the cobweb. Note that the purple cycle shown is computed by simulating the full model. In that case, model variables may have slightly different values compared to the ones obtained from map initial conditions, thus, leading to slight differences in computed phase values

pattern), corresponding to another period doubling. Across the interval  $\chi \in [0.8585, 0.866]$  we numerically detect an apparent period doubling cascade. As shown in Fig. 5, the  $\rho_{REM}=4$  regime ends at  $\chi=0.8545$  with a  $\{1_4,1_4,1_4\}^\infty$  solution.

With the decrease in  $\chi$ , changes to the sleep onset circle maps reflect changes in potential transient solutions as well as the stable solutions. In addition to the shifts of the map that drive many of the changes in stable solutions, the shapes of the map branches change and some branches are lost which can affect the transient solutions that may occur in the model. Since sleep need accumulates and dissipates at a higher rate with lower  $\chi$ , the duration of sleep episodes is shorter and the total number of REM bouts that can occur during the sleep episode decreases. For example, for  $\chi \sim 0.86$ , the branch associated with eight REM bouts no longer exists. This reflects the loss of transient solutions that involve sleep episodes with eight REM bouts.

 $\rho_{REM} \in (4,5)$ 

As  $\chi$  continues to decrease, the map evolves further such that stable orbits visit the map branch involving sleep episodes with five REM bouts (Fig. 7, red branch). Stable solutions consist of higher order cycles where sleep onset phases alternate between points on the four-REM-and five-REM-branches of the map. For example, at  $\chi=0.8535$  the stable solution  $\{1_4,1_4,1_4,1_4,1_5\}^\infty$  is detected. These higher order cycles follow a period-adding-type sequence as  $\chi$  decreases with the number of sleep episodes with 4 REM bouts decreasing incrementally with each stable solution. In the interval  $\chi\in[0.811,0.8375]$ , the stable solution is  $\{1_4,1_5\}^\infty$  with  $\rho_{REM}=4.5$ , and for lower  $\chi$  values the number of sleep episodes with 5 REM bouts in the pattern increases incrementally as  $\rho_{REM}$  approaches 5. Within this period-adding-type sequence, we detected some period-doubling transitions where the same pattern of sleep episodes and REM bouts is repeated twice with slight variation in the phases of sleep and REM onsets.

As shown in the  $\rho_{REM}$  bifurcation diagram (Fig. 5), the  $\{1_5\}^\infty$  solution with  $\rho_{REM}=5$  gains stability at  $\chi\approx0.786$  where higher order cycles also are stable, leading to an interval of bistability in the system. Interestingly, the structure of the map predicts the existence of the two stable solutions that are associated with distinct sets of stable and unstable fixed points on the map (Fig. 7A). Specifically, the higher order cycles  $\{1_4,\ldots,1_4,1_5,\ldots,1_5\}^\infty$  manifest on the map as an orbit that moves between the left side of the four-REM-branch (green) and the right side of the five-REM-branch (red). In contrast, the  $\{1_5\}^\infty$  solution first appears when the left side of the five-REM-branch (red) makes a tangent intersection with the  $\Phi_{n+1}=\Phi_n$  diagonal,

 $\rho_{REM} = 5$ 

The  $\{1_5\}^{\infty}$  solution is stable in the interval  $\chi \in [0.773, 0.786]$  (Fig. 5). The stable fixed point associated with this solution corresponds to sleep onset phases on the left side of the five-REM-branch that represent earlier phases compared to the phases that participate in the higher order cycle. The  $\{1_5\}^{\infty}$  solution loses stability when the slope of the branch at this fixed point decreases below -1. In the narrow interval  $\chi \in [0.7805, 0.7815]$ , we found numerical evidence for a period-doubling cascade involving  $\{1_5, \dots, 1_5\}^{\infty}$  solutions.

 $\rho_{REM} \in (5,6]$ 

The bifurcation sequence associated with the appearance of sleep episodes with 6 REM bouts is similar to the sequence described for the sleep episodes with 5 REM bouts. Specifically, as  $\chi$  decreases from 0.773, we find stable higher order cycles with sleep onset phases alternating between the 5-REM- (red branch) and 6-REM-branches (light blue branch) of the map (Fig. 7B). These stable orbits form a period-adding-type sequence as  $\chi$  decreases with the number of sleep episodes containing 5 REM bouts decreasing until the  $\{1_5, 1_6\}^{\infty}$  solution is obtained at  $\chi = 0.7595$ . At the higher value  $\chi = 0.765$ , the stable solution  $\{1_6\}^{\infty}$  with  $\rho_{REM}=6$  appears for the first time when the six-REM-branch of the map intersects the diagonal  $\Phi_{n+1} = \Phi_n$  at a saddle-node bifurcation. As above, the bistable solutions correspond to different sets of stable and unstable fixed points on the map. The stable fixed point of the stable-unstable fixed point pair on the left side of the six-REM-branch is associated with the  $\{1_6\}^\infty$  solution, while the sleep onset phases of the higher order orbits alternate between the right side of the six-REM-branch and the left side of the five-REM-branch (Fig. 7B, inset). There are also 2 unstable fixed points near the right end of the five-REM-branch and the left end of the four-REM branch, however,

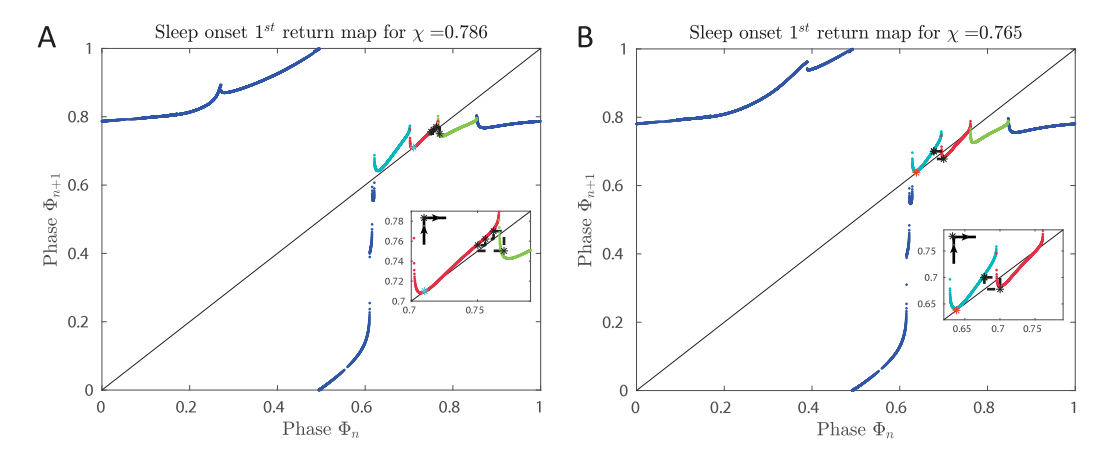


Fig. 7. First return maps in the  $\rho=1$  regime designating the onset of the  $\rho_{REM}=5$  and  $\rho_{REM}=6$  solutions. The green, red and light blue map branches correspond to circadian phases of sleep episodes involving 4, 5, and 6 REM bouts, respectively. A. First return map for  $\chi=0.786$  showing bistability of solutions with  $4<\rho_{REM}<5$  and  $\rho_{REM}=5$ . The light blue asterisk (at  $(\Phi_n,\Phi_{n+1})=(0.71,0.71)$  on the red branch) indicates the onset of the stable  $\rho_{REM}=5$  solution in a saddle-node bifurcation. This solution coexists with a higher order cycle of  $\rho_{REM}=\frac{19}{2}$  illustrated on the map (inset, black arrows indicate the direction of the cycle through a point (asterisk) that lies above the diagonal). Cobwebbing on the map produces approximately the same cycle. B. The first return map for  $\chi=0.765$  showing bistability of solutions with  $5<\rho_{REM}<6$  and  $\rho_{REM}=6$ . The red asterisk (at  $(\Phi_n,\Phi_{n+1})=(0.6379,0.6379)$  on the light blue branch) indicates the onset of the stable  $\rho_{REM}=6$  solution in a saddle-node bifurcation. This solution coexists with a higher order cycle of  $\rho_{REM}=\frac{1}{2}$  illustrated on the map (inset, black arrows indicate the direction of the cycle through a map point (asterisk) that lies above the diagonal). Cobwebbing on the map produces approximately the same cycle.

we did not numerically detect any stable higher order orbits near those points.

### Summary

In summary, we have shown that in the  $\rho=1$  regime of monophasic sleep in the three-state model, NREM–REM alternation introduces a sequence of bifurcations as  $\chi$  is reduced. These bifurcations correspond to changes in the timing and number of REM bouts during the single nocturnal sleep episode and reflect interactions between NREM–REM alternation and sleep—wake dynamics. These results suggest the potential for developmental changes in ultradian alternation during sleep after consolidation to a single nocturnal sleep episode.

The sequence of bifurcations is initiated by a loss of stability in the  $\{1_4\}^{\infty}$  solution and include period-adding-type patterns in the numbers of REM bouts and bistability at the transitions to the  $\{1_5\}^{\infty}$  and  $\{1_6\}^{\infty}$ solutions. Specifically, the  $\{1_n\}^{\infty}$  (n = 4, 5) solutions lose stability in period-doubling bifurcations when the slope of the map at the stable fixed point decreases below -1 because of the non-monotonic shape of the map branches. For n = 4, 5, period-doubling solutions with nREM bouts are replaced by solutions involving daily sleep episodes with n and n + 1 REM bouts that follow a period-adding sequence. These higher order stable orbits display sleep onset phases near an unstable fixed point on the map. The stable solutions  $\{1_n\}^{\infty}$  (n =5,6) are initiated at saddle-node bifurcations which introduce stable and unstable fixed points on the map. These saddle-node bifurcations occur at  $\chi$  values where the higher-order cycle solutions retain stability leading to intervals of bistability near these bifurcations. The unstable fixed point associated with higher order cycling between  $\{1_4\}^{\infty}$  and  $\{1_5\}^{\infty}$  solutions is eventually lost through a border collision bifurcation.

Interestingly, this same sequence of bifurcations is not followed in the evolution and finally disappearance of the  $\{1_6\}^\infty$  solution at  $\chi=0.7235$ . As  $\chi$  is reduced from 0.765 (where the  $\{1_6\}^\infty$  solution gains stability in a saddle–node bifurcation), the six-REM-branch shrinks to cover a narrower interval of circadian phases but the stable and unstable fixed points remain on the branch. At  $\chi=0.7235$ , the lowest  $\chi$  value where the  $\rho=1$  solution exists, the stable and unstable fixed points on the six-REM-branch coalesce in a saddle–node bifurcation leading to the loss of the  $\{1_6\}^\infty$  solution (Fig. 8B). Additional occurrences of bistability appear near this bifurcation where at the slightly higher  $\chi$  value of  $\chi=0.726$  we find a stable higher order orbit with  $\rho=\frac{4}{5}$ ,  $\rho_{REM}=\frac{20}{5}=4$ , and a pattern of  $\{1_5,1_5,1_3,2_{(4,3)}\}^\infty$  (Fig. 8A). Thus, near where the  $\rho=1$  solutions lose stability, the period-adding

solutions in the number of sleep episodes per circadian cycle start to appear. Such bistability between these types of solutions has not been observed in two-state sleep–wake models (see Discussion). The first return map eventually deforms so that the six-REM-branch vanishes, as at  $\chi=0.7165$  (Figure 14B in Supplementary Material), while the two neighboring five-REM branches merge into a single branch. As a result, stable or transient solutions involving sleep episodes with six REM bouts are not predicted by the map for this value of  $\chi$ .

### 3.2. Effects of NREM-REM cycling on the monophasic to biphasic sleep transition

The loss of existence of the  $\rho = 1$  solution designates the appearance of circadian cycles with two sleep episodes (e.g., nap and nighttime sleep). As  $\chi$  decreases through the transition from stable monophasic to stable biphasic sleep, the  $\rho$  bifurcation diagram reflects an underlying period adding structure (Figs. 4B and 9A). However, in some  $\chi$  intervals the monotonic change in  $\rho$  characterizing the period adding structure is disrupted (Fig. 9A). Specifically, the sequence of rotation numbers  $\rho$  is irregular and non-monotonic at high values of  $\chi$  in this region ( $\chi \in (0.7015, 0.7235)$ ) and exhibits jumps within particular  $\rho$ -intervals resulting in bistability. For example, at  $\chi = 0.6305$  stable solutions  $\rho = \frac{2}{3}$  and  $\rho = \frac{13}{19}$  both exist. Additionally, bistability is observed at the transition between distinct  $\rho$  values. For example, for  $\chi \in [0.659, 0.661]$  stable solutions with  $\rho = \frac{7}{10}$  (with  $\rho_{REM} = 3.4$ ) and  $\rho = \frac{2}{3}$  (with  $\rho_{REM} = 3$ ) coexist (right end of pink shaded region in Fig. 9A). Such irregularity in sleep pattern changes in this regime suggests that the developmental change from a napping to a non-napping sleep schedule in young children can involve a wide range of multi-day sleep patterns before consistent monophasic sleep is achieved.

Variations in NREM–REM cycling contribute to the irregularity of variation in  $\rho$  as  $\chi$  decreases, as illustrated in the  $\rho_{REM}$  bifurcation diagram (Fig. 9B). In this section, we qualitatively describe characteristics of the diversity of solutions in the transition from monophasic to biphasic sleep since stable solutions with  $\rho \in (\frac{1}{2},1)$  are represented in higher order return maps that are quite complex. In the next section, we discuss bifurcation sequences more quantitatively and show second return maps for the  $\rho = \frac{1}{2}$  solutions.

### Diversity of NREM-REM cycling for solutions with constant $\rho$

In  $\chi$  intervals of constant  $\rho$  for  $\rho \in (\frac{1}{2}, 1)$ , changes in  $\rho_{REM}$  may or may not follow a monotonic period-adding-type sequence with

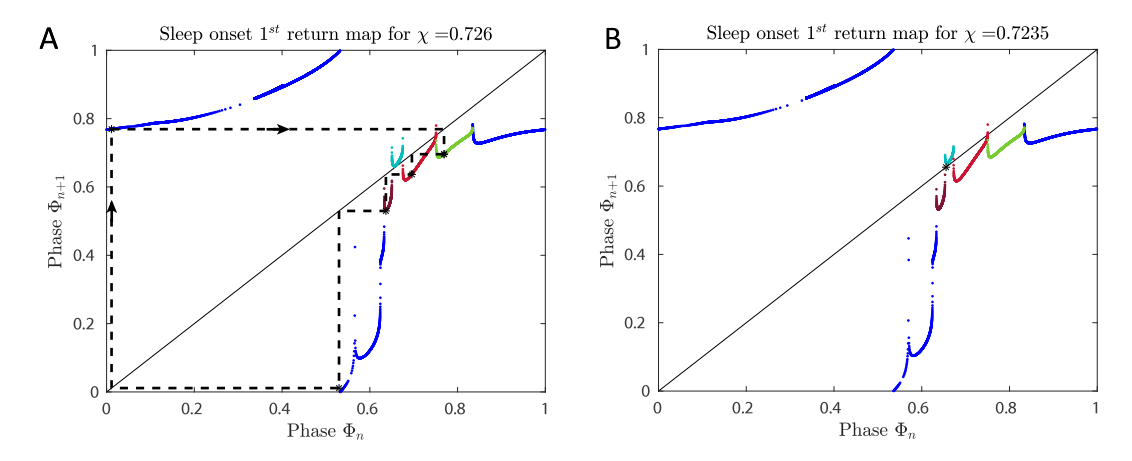


Fig. 8. First return maps toward the end of the  $\chi$  range for the stable  $\rho=1$  solution. The green, red, light blue map, and purple branches correspond to circadian phases of sleep episodes involving 4, 5, 6, and 5 REM bouts, respectively. A. The first return map for  $\chi=0.726$  showing the stable solution with  $\rho<1$  ( $\{1_5,1_5,1_3,2_{(4,3)}\}^\infty$ ) in a bistable regime with the  $\{1_6\}^\infty$  solution (stable fixed point on the light blue branch). The stable solution with  $\rho<1$  visits the five-REM (purple and red), four-REM (green) and three-REM (dark blue) branches. Black arrows along the dashed lines indicate the direction of the cycle. Cobwebbing on the map produces approximately the same cycle. B. The first return map for  $\chi=0.7235$ . The  $\rho=1$  solution ceases to exist in a saddle-node bifurcation on the six-REM branch (light blue).

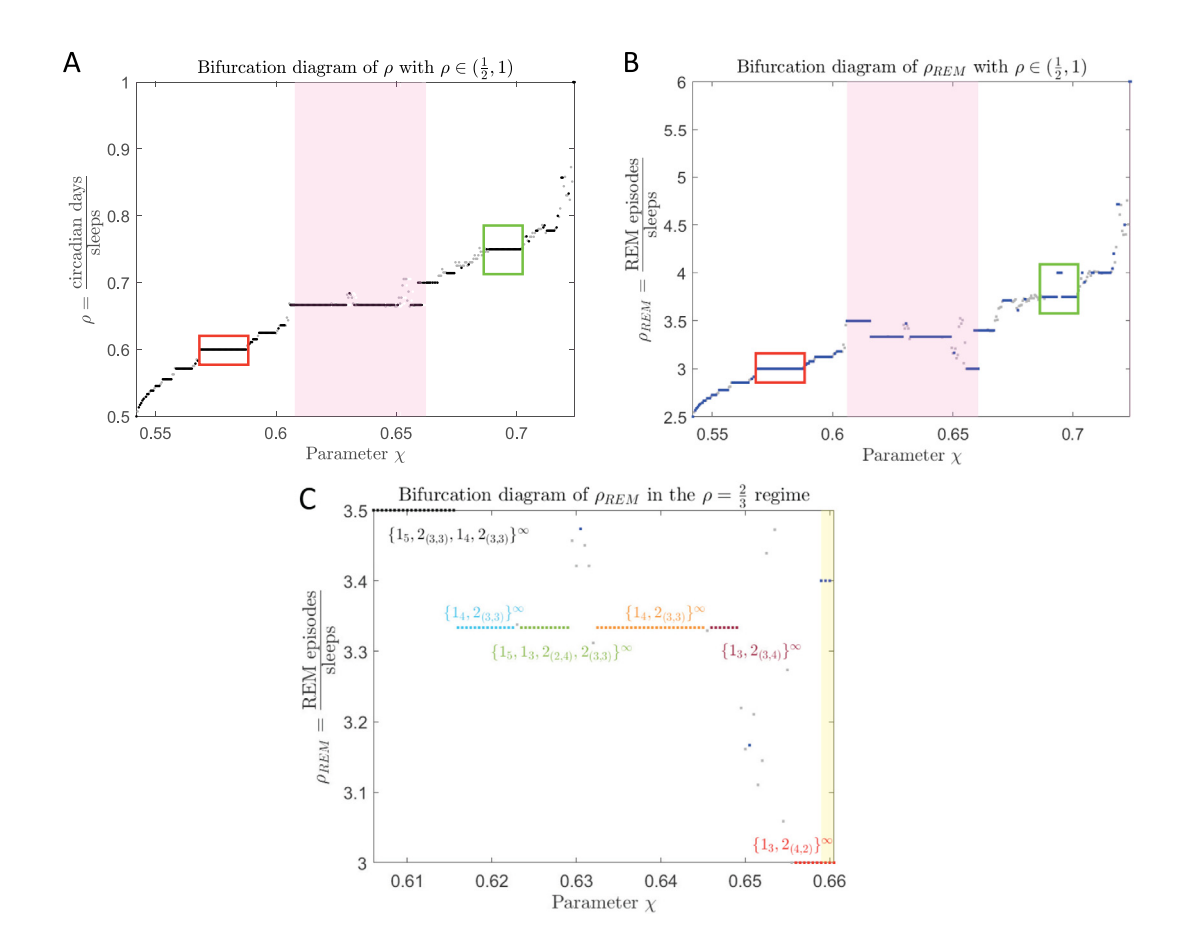
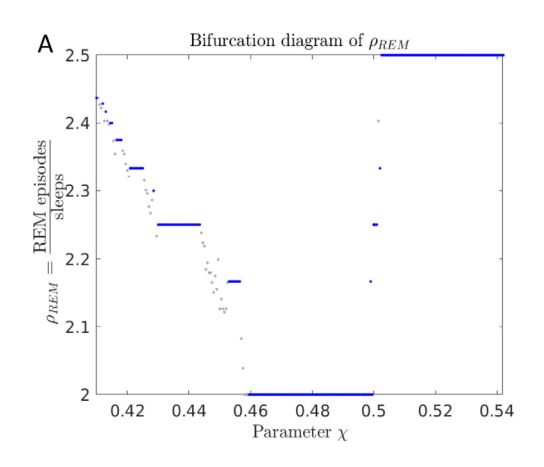


Fig. 9. Bifurcation diagrams of  $\rho$  and  $\rho_{REM}$  in the transition from monophasic to polyphasic sleep. A,B: Bifurcation diagram of  $\rho$  (A) and  $\rho_{REM}$  (B) with  $\rho \in (\frac{1}{2}, 1)$ . Pink shaded regions indicate the  $\chi$  interval where the majority of solutions have  $\rho = \frac{2}{3}$ . Green and red boxes correspond to stable solutions with  $\rho = \frac{3}{4}$  for  $\chi \in [0.6875, 0.7015]$  and with  $\rho = \frac{3}{5}$  for  $\chi \in [0.5685, 0.5875]$ , respectively. These  $\chi$  intervals illustrate the diversity of  $\rho$  and  $\rho_{REM}$  variations as  $\chi$  decreases caused by variations in NREM-REM cycling. C:  $\rho_{REM}$  bifurcation diagram for  $\chi \in [0.606, 0.6605]$  corresponding to an average sleep pattern of three sleeps per two days (i.e.  $\rho = \frac{2}{3}$ ). The light yellow shaded region indicates an interval of bistability of stable solutions with  $\rho = \frac{7}{10}$  and  $\rho = \frac{2}{3}$ . Intervals of constant  $\rho_{REM}$  are colored and labeled appropriately with the particular sleep pattern. Each subinterval may involve a period doubling bifurcation which is not labeled.

decreasing  $\chi$  as observed for  $\rho=1$  solutions. For example, for  $\chi\in[0.5685,0.5875]$  (red box in Fig. 9A,B) all stable solutions have  $\rho=\frac{3}{5}$  and  $\rho_{REM}=3$  corresponding to the pattern  $\{1_3,2_{(2,4)},2_{(3,3)}\}^{\infty}$ . Similarly,

for all solutions in  $\chi \in (0.542, 0.606)$ , solutions with the same  $\rho$  value have a consistent  $\rho_{REM}$  value. In contrast, for solutions with  $\rho = \frac{3}{4}$ , for  $\chi \in [0.6875, 0.7015]$  (green box in Fig. 9A,B),  $\rho_{REM}$  jumps from 3.75 to



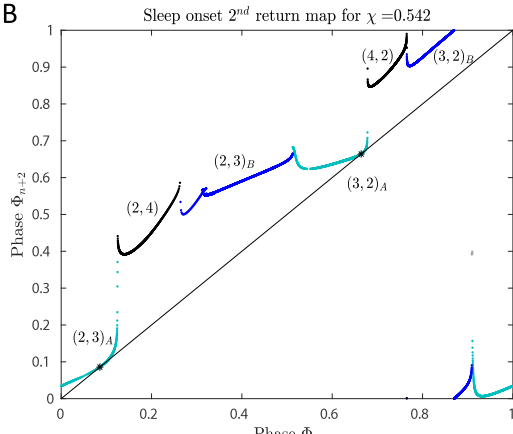


Fig. 10. The biphasic sleep ( $\rho = \frac{1}{2}$ ) regime. A. The bifurcation diagram of  $\rho_{REM}$  in the  $\rho = \frac{1}{2}$  regime. B. The second return map for  $\chi = 0.542$  introducing the  $\rho = \frac{1}{2}$  solution in a saddle–node bifurcation. The stable solution has  $\rho_{REM} = 2.5$ . The map branches are colored and labeled according to the number of REM bouts involved in the sleep onsets with phase  $\Phi_n$  and  $\Phi_{n+1}$ . The dark blue and light blue branches correspond to model solutions having 2 and 3 REM bouts during the two sleep episodes, respectively. The black branches correspond to solutions with 2 and 4 REM bouts during the two sleep episodes, respectively.

4 for  $\chi \in [0.6935, 0.695]$  indicating a difference in NREM–REM cycling patterns in solutions with the same  $\rho$ .

$$\rho = \frac{2}{3}$$

As a further example, the bifurcation diagram of  $\rho_{REM}$  over the interval  $\chi \in [0.606, 0.6605]$  (Fig. 9C) illustrates the diversity of NREM-REM cycling patterns that occur in  $\rho = \frac{2}{3}$  solutions. Here,  $\rho_{REM}$ values generally increase in a period-adding-type sequence. In the range  $\chi \in [0.617, 0.649]$ ,  $\rho_{REM} = \frac{10}{3}$  and reflects a stable pattern with an average number of 10 REM bouts per 3 sleep episodes. However, the distribution of REM bouts across the 3 sleep episodes varies with  $\chi$  and results in four distinct stable sleep patterns across this range. At  $\chi = 0.649$ , the stable sleep pattern is  $\{1_3, 2_{(4,3)}\}^{\infty}$ , but at  $\chi = 0.645$ the pattern changes to  $\{1_4,2_{(3,3)}\}^{\infty}$ . This change occurs due to a phase advance of the second sleep episode with 3 REM bouts that eventually shifts it to the previous circadian day. For lower  $\chi$  values, NREM-REM cycling patterns change, leading to variable  $\rho_{REM}$  that then re-stabilizes at  $\chi = 0.6235$  where the stable sleep pattern is  $\{1_5, 1_4, 2_{(4,2)}, 2_{(3,3)}\}^{\infty}$ . Period doubling bifurcations take place for  $\chi \in [0.6235, 0.6245]$  and at  $\chi=0.6225$  the pattern becomes  $\{1_4,2_{(3,3)}\}^\infty$  (no stable solutions were detected for  $\gamma \in (0.6225, 0.6235)$ ). This representative example emphasizes the great range of NREM-REM cycling patterns predicted by the three-state model.

An additional example of this range of patterns is highlighted by the re-occurrence of some  $\rho_{REM}$  values over distinct  $\chi$  intervals (e.g.,  $\rho_{REM}=3$  for  $\chi\in[0.5685,0.5875]\cup[0.656,0.6605]$ ). In this example, the  $\chi$  intervals correspond to distinct sleep patterns that are characterized by different  $\rho$  values despite having the same average number of REM bouts per sleep episode. However, re-occurrence of  $\rho_{REM}$  values can take place even within the same  $\rho$  interval. This phenomenon, as well as the map structure leading to it, is illustrated in the next section.

### 3.3. NREM-REM cycling bifurcations in biphasic sleep

Stable biphasic sleep  $(\rho=\frac{1}{2})$  solutions occur for  $\chi\in[0.41,0.542]$ . NREM-REM cycling changes across this regime, with  $\rho_{REM}$  varying non-monotonically in  $\rho_{REM}\in[2,2.5]$  (Fig. 10A). This non-monotonic variation in  $\rho_{REM}$  with  $\chi$  is due to more variability in NREM-REM cycling patterns across the two daily sleep episodes, as described in the previous section for  $\rho=\frac{2}{3}$  solutions. Such variability suggests

that the biphasic sleep pattern can accommodate changes in NREM-REM alternation that alter the specific timing, duration, and REM sleep content of naps and nighttime sleep without affecting the number of daily sleep episodes. To analyze the bifurcation sequences occurring in this regime, we employ second return maps and follow the  $\rho_{REM}$  bifurcation diagram (Fig. 10A) as  $\chi$  is reduced from 0.542.

Note that the second return map can be thought of as consisting of two similar copies of the map branches (Fig. 10B). Each pair of associated branches involves the same set of model trajectories that produce two sleep episodes. One branch represents the sleep onset phases of the first sleep episode of the day, while the associated branch represents the sleep onset phase of the second sleep episode of the day.

### $\rho_{REM} = 2.5$

The  $\rho = \frac{1}{2}$  regime is initiated at  $\chi = 0.542$  in a saddle-node bifurcation illustrated in the second return map (Fig. 10B). This map has two fixed points at phases about  $\Phi_n = \Phi_{n+2} = 0.0857$  and  $\Phi_n =$  $\Phi_{n+2} = 0.6641$  formed by map branches (light blue) making tangential intersections with the diagonal. Thus, at the start of the  $\rho = 1/2$  regime, the stable periodic orbit consists of a sleep episode with two REM bouts occurring at the early rise of the circadian rhythm (near  $\Phi_n = 0.0857$ ) followed by a sleep episode with three REM bouts occurring a little after the peak of the circadian rhythm (near  $\Phi_n = 0.6641$ ). This results in a REM rotation number,  $\rho_{REM} = 2.5$ . We refer to the branches on which the fixed points lie as the  $(2,3)_A$  (near  $\Phi_n = 0.0857$ ) and  $(3,2)_A$  (near  $\Phi_n = 0.6641$ ) branches. The first number in the 2-tuple of a map branch refers to the number of REM bouts occurring in the sleep episode with onset phase,  $\Phi_n$ . The second number refers to the number of REM bouts in the subsequent sleep episode with onset phase,  $\Phi_{n+1}$ . The subscripted letters distinguish between distinct, map branches corresponding to model solutions exhibiting the same numbers of NREM-REM cycles.

As  $\chi$  decreases from the value  $\chi=0.542$  associated with the saddle-node point, the second return map attains two pairs of fixed points, one pair from each saddle-node with a stable and an unstable fixed point in each pair. The slope of the map branches at the stable fixed points is initially positive and less than 1, but as  $\chi$  decreases, it becomes negative and eventually decreases through -1 at approximately  $\chi=0.503$ , indicating a period-doubling bifurcation. When the stable fixed points lose stability at  $\chi=0.5025$ , a stable 4-cycle emerges with the pattern  $\{2_{(2,3)}, 2_{(2,3)}\}^{\infty}$ . On the second return map (Fig. 11A), the 4-cycle appears as two 2-cycles, one with sleep onset phases on the

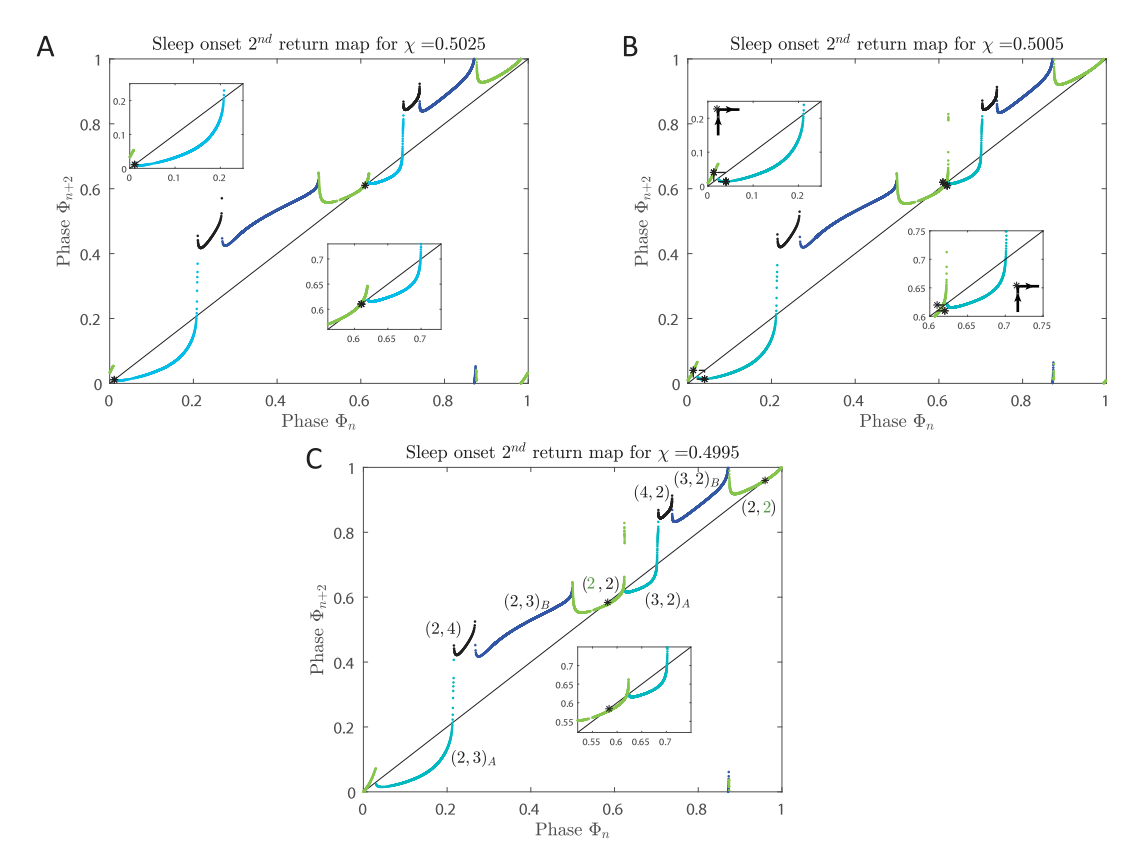


Fig. 11. Higher order cycling solutions in the  $\rho = \frac{1}{2}$  regime represented in the second return maps. The two insets in panels A and B show the 2-cycles associated with the sleep onsets in the stable solution occurring at earlier and later circadian phases. The behavior is qualitatively the same, thus we show only one inset in the remaining figures. Black arrows in the insets of panel B indicate the direction of the cycle through a point (asterisk) that lies above the diagonal. Cobwebbing on the map produces approximately the same cycle. The map branches are labeled according to the number of REM bouts involved in the sleep onsets with phase  $\Phi_n$  and  $\Phi_{n+1}$  in panel C. The light and dark blue, black and green branches correspond to model solutions involving 2 and 3, 2 and 4, and 2 and 2 REM bouts during their first two sleep episodes, respectively. A. Second return map for  $\chi = 0.5025$  in the  $\rho_{REM} = 2.5$  regime. The stable solution is characterized by higher order cycles after a period doubling bifurcation. B. Second return map for  $\chi = 0.4995$  in the  $\rho_{REM} = 2$  regime. A saddle-node bifurcation introduces the stable solution with pattern  $\{2_{(2,2)}\}^{\infty}$ .

 $(2,3)_A$  branch (light blue) near  $\Phi_n \approx 0$  and the other with phases on the  $(3,2)_A$  branch (light blue) near  $\Phi_n \approx 0.6$ . The sleep onset phases of the sleep episodes are almost equal. Note that the unstable fixed points still exist on the right side of these map branches.

### $\rho_{REM}=2.25$

As  $\chi$  decreases a little further to  $\chi \in [0.5005, 0.501]$ ,  $\rho_{REM}$  decreases to 2.25, and the stable solution transitions to the pattern  $\{2_{(2,2)}, 2_{(2,3)}\}^{\infty}$ . In this solution, sleep onset phases alternate between neighboring map branches  $(2,3)_A$  (or  $(3,2)_A$ , light blue) and (2,2) (green) which appeared during the evolution of the map with  $\chi$  (Fig. 11B). Unlike the bifurcation sequences seen in the  $\rho=1$  regime, where higher order cycle solutions consisting of sleep onset phases on two distinct map branches follow a period-adding-type sequence, here only the  $\{2_{(2,2)}, 2_{(2,3)}\}^{\infty}$  pattern  $(\rho_{REM}=2.25)$  persists with an abrupt transition to the  $\{2_{(2,2)}\}^{\infty}$  solution  $(\rho_{REM}=2)$  (Fig. 10A). This abrupt transition occurs in a border collision bifurcation at  $\chi=0.5005$  when the  $(2,3)_A$  and  $(3,2)_A$  (light blue) map branches intersect the diagonal,  $\Phi_{n+2}=\Phi_n$ , at the unstable fixed points lying on their leftmost side (Fig. 11B).

### $\rho_{REM} = 2$

The stable  $\{2_{(2,2)}\}^{\infty}$  solution is found at approximately  $\chi=0.4995$  as a result of a pair of saddle–node bifurcations via a tangent intersection of both (2,2) (green) map curves with the diagonal (Fig. 11C). The saddle–node bifurcation creates two pairs of stable and unstable fixed points, one pair on each (2,2) map branch. As before, as  $\chi$  decreases further, the slope of map branches at the stable fixed points eventually

decreases through -1 at  $\chi=0.462$  leading to a period-doubling bifurcation.

### Evolution of map branches

Note that during this evolution of decreasing  $\chi$ , the shape of the second return map has significantly changed compared to its structure at  $\chi=0.542$  (Fig. 10B). In particular, for  $\chi=0.542$  the (2,4) and (4,2) branches existing on phase intervals  $\Phi_n\in(0.1242,0.2624)$  and  $\Phi_n\in(0.6778,0.764)$ , respectively, correspond to trajectories that generate sleep episodes involving four REM bouts (Fig. 10B, black curves). As  $\chi$  is reduced, and the faster variation in homeostatic sleep drive decreases the duration of sleep episodes, the total number of REM bouts during a sleep episode decreases as well. The map reflects this phenomenon as the (2,4) and (4,2) branches exist over narrower  $\Phi_n$  intervals for decreasing  $\chi$ . These branches are eventually annihilated, while their neighboring (2,3) $_A$ , (2,3) $_B$ , (3,2) $_A$ , (3,2) $_B$  branches on either side merge into continuous S-shaped (2,3) and (3,2) curves (Fig. 12).

### Reoccurrence of solutions with $\rho_{REM} > 2$

For  $\chi < \approx 0.4875$ , the second return map comprises curves that correspond to sleep cycles that involve only two or three REM bouts (Fig. 12A). Stable period doubling orbits are obtained on the (2,2) (green) branches of the map for  $\chi \in [0.4595, 0.462]$  (Fig. 12B). For lower  $\chi$  values, we obtain more stable higher order cycle solutions with sleep onset phases alternating between distinct map branches. Specifically, at  $\chi = 0.4565$ , a stable 6-cycle with the pattern of  $\{2_{(2,3)}, 2_{(2,2)}, 2_{(2,2)}\}^{\infty}$  is observed with sleep onset phases on the (2,2) (green) and on the

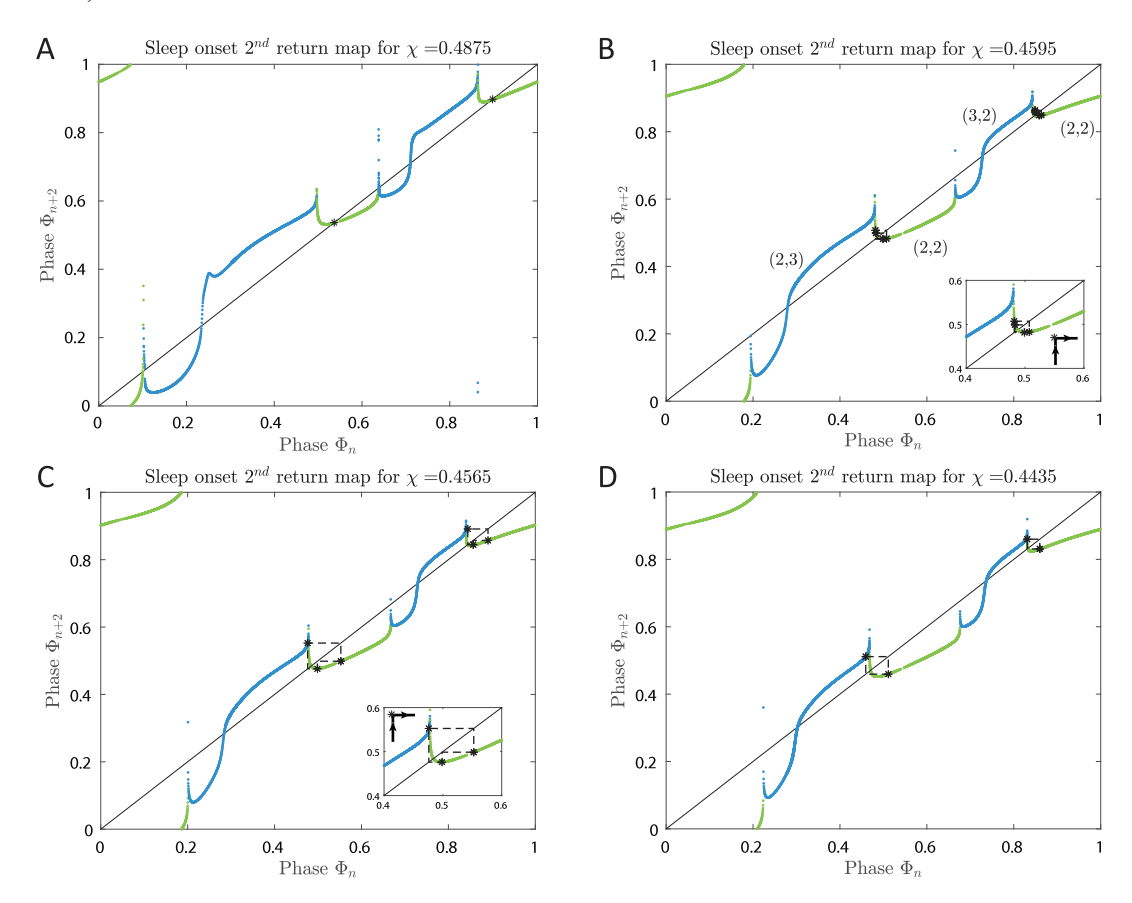


Fig. 12. Second return maps capturing  $\rho=\frac{1}{2}$  solutions with only two or three REM bouts per sleep episode. The maps deform and comprise only four branches corresponding to a distinct number of REM bouts. The map branches are labeled and colored according to the number of REM bouts involved in the sleep onsets with phase  $\Phi_n$  and  $\Phi_{n+1}$  in panel B. The light blue and green branches correspond to model solutions involving 2 and 3, and 2 REM bouts during the two sleep episodes, respectively. Black arrows in the insets of panels indicate the direction of the cycle through a point (asterisk) that lies above the diagonal. Cobwebbing on the map produces approximately the same cycle. A. Second return map for  $\chi=0.4875$  exhibiting the annihilation of the branches involving sleep onset phases with four REM bouts. B. Second return map for  $\chi=0.4875$  exhibiting the annihilation. C. Second return map for  $\chi=0.4875$ . The stable solution has  $\rho_{REM}=\frac{13}{6}$  manifesting the monotonic increase of  $\rho_{REM}$  as  $\chi$  is reduced. D. Second return map for  $\chi=0.4435$ . The stable solution has  $\rho_{REM}=\frac{13}{6}$  manifesting the monotonic increase of  $\rho_{REM}$  as  $\chi$  is reduced. D. Second return map for  $\chi=0.4435$ . The stable solution has  $\rho_{REM}=\frac{1}{2}$  and alternates between the (2,3) (or (3,2)) and (2,2) map branches.

S-shaped (2,3) (or (3,2)) (blue) branches (Fig. 12C). This pattern corresponds to  $\rho_{REM}=\frac{13}{6}$  and loses stability at  $\chi=0.453$  where the higher order pattern  $\{2_{(2,3)},2_{(2,2)},2_{(2,2)},2_{(2,3)},2_{(2,2)},2_{(2,2)}\}^{\infty}$  occurs. As  $\chi$  decreases further, the stable sleep patterns visit the (2,2) (green) map branches less frequently and visit the (2,3) (or (3,2), blue) branches more frequently. Thus, the REM rotation number starts increasing incrementally from 2 in a period-adding type fashion.

As  $\chi$  values approach the lower end of the  $\rho=\frac{1}{2}$  regime, the  $\rho_{REM}=2.25$  solution with pattern  $\{2_{(2,3)},2_{(2,2)}\}^{\infty}$  is introduced once more for  $\chi\in[0.43,0.4435]$  (Fig. 12D). In this occurrence of the solution, the phases of sleep episodes have shifted to the second half of the circadian day. That is, the earlier sleep onsets occur close the peak of the circadian rhythm and the later ones occur close to the trough of the circadian rhythm. As  $\chi$  decreases further, we numerically detect a period doubling cascade from the  $\{2_{(2,3)},2_{(2,2)}\}^{\infty}$  pattern for  $\chi\in[0.43,0.431]$  (Figure 15A in Supplementary Material).

Finally, as  $\chi$  decreases out of the  $\rho=\frac{1}{2}$  regime, the REM rotation number,  $\rho_{REM}$ , keeps increasing incrementally reflecting a period-adding-type sequence as more days with  $2_{(2,3)}$  sleep cycles are added to the pattern with  $2_{(2,2)}$  days. In the map, this translates to more phase onsets in the higher order cycles lying on the S-shaped (2,3) and (3,2) (blue) branches. At  $\chi=0.41$ , a border collision at the unstable fixed points on each of the (2,2) (green) map branches designates the loss of stability of the  $\rho=\frac{1}{2}$  solution (Figure 15B in Supplementary Material). Given the structure of the map branches, no stable fixed points exist in the second return map and no higher order cycles can be created. As a result, sleep patterns with days involving three sleep episodes emerge.

### Summary

In summary, the bifurcation sequence in the  $\rho=\frac{1}{2}$  regime displays similarities with the  $\rho=1$  regime, including period doubling when fixed points lose stability due to a change in the slope of the map branch at the fixed point, creation of stable fixed points through saddle–node bifurcations, and higher order cycling solutions with period-adding-type patterns in  $\rho_{REM}$  involving sleep onset phases on distinct map branches. However, by contrast with the  $\rho=1$  regime, a large portion of the  $\rho=\frac{1}{2}$  regime involves solutions that are higher order cycles around unstable fixed points. Thus, this regime shows many occurrences of the loss of unstable fixed points through border collision bifurcations governing the transitions in solution patterns. The presence of stable higher order cycles, rather than stable fixed points, may have implications for re-entrainment dynamics for regularly napping children experiencing a perturbation to their typical schedule.

Additionally, certain  $\rho_{REM}$  solutions in the interval [2,2.5] re-occur at different  $\chi$  values. However, the size of the  $\chi$ -interval for each occurrence of  $\rho_{REM}$  differs due to the asymmetrical shape of the map branches. Specifically, the higher order cycling solutions exist over larger  $\chi$  values when the unstable fixed point that they surround lies on the left side of the map branch that has a longer vertical distance from its border associated with the cusp.

The stable solutions generated for smaller  $\chi$  values in this regime capture the sleep patterns and timing observed in napping children. In particular, the phase of the earlier sleep onset occurs close to the peak of the circadian drive (midday nap, Fig. 12) as reported in experimental studies [54]. Additionally, the values of the homeostatic time constants

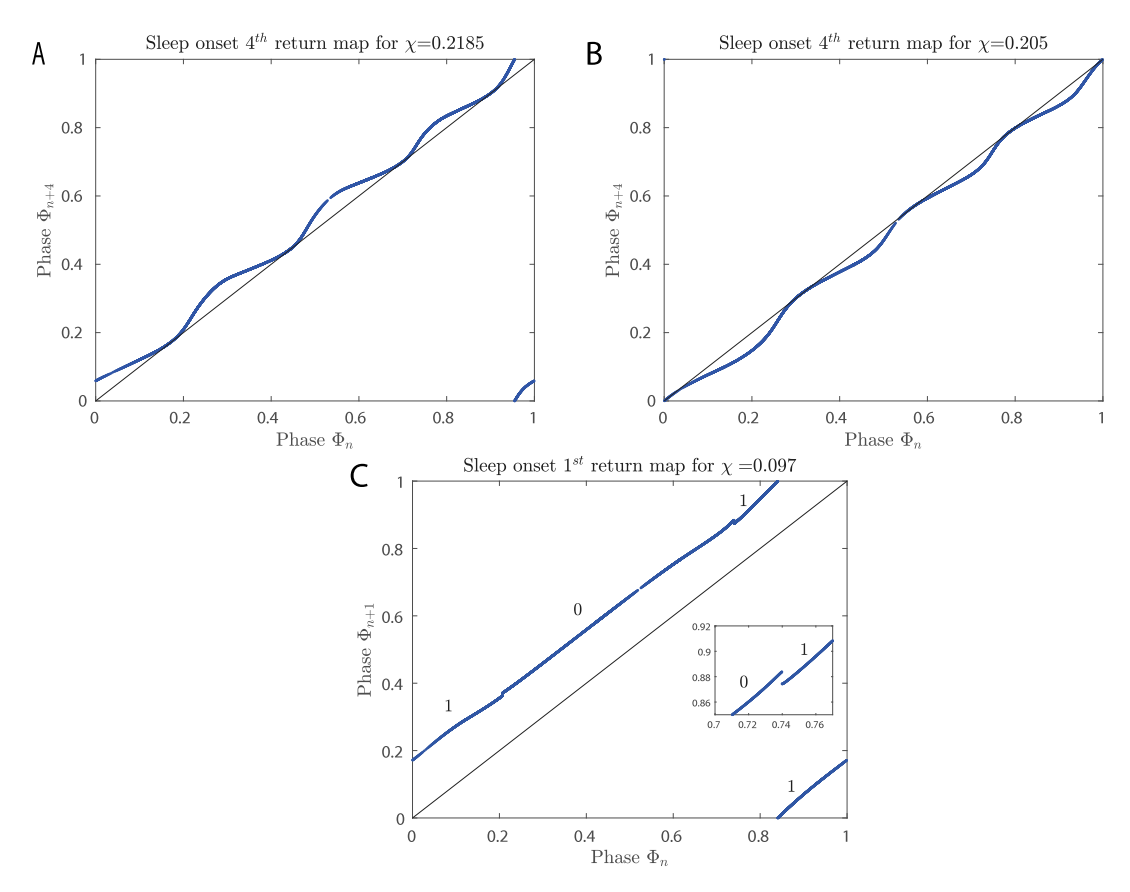


Fig. 13. Maps showing the transition from a continuous to a discontinuous regime for small  $\chi$ . A. The fourth return map for  $\chi=0.2185$  designates the beginning of the  $\rho=\frac{1}{4}$  solution. The map is continuous in this regime, and thus, the stable solution emerges in a saddle–node bifurcation. B. The fourth return map for  $\chi=0.205$  demonstrating the loss of existence of the  $\rho=\frac{1}{4}$  solution. The map remains continuous and thus, the stable solution ceases to exist in a saddle–node bifurcation. C. The first return map for  $\chi=0.097$ . Occurrence of solutions with one or no REM bouts due to the fast time scales of the homeostatic sleep drive lead to the reappearance of discontinuities in the map. Each discontinuity exists to differentiate between map branches that correspond to sleep episodes with different number of REM bouts. The branches are labeled according to the number of REM bouts involved in the initial sleep occurring at phase,  $\Phi_n$ .

are consistent with experimentally estimated values [55]. Further data on typical REM sleep timing and patterns observed in young children as they transition from napping to non-napping sleep schedules is needed to validate and constrain model predictions for other ranges of  $\chi$  values. Such data will help to more accurately understand the effect of changing properties of the sleep homeostat on sleep patterns in early childhood.

### 3.4. Loss of NREM-REM cycling in the polyphasic sleep limit

The loss of existence of the  $\rho=\frac{1}{2}$  solution initiates the appearance of circadian cycles with three sleep episodes (e.g., morning nap, afternoon nap, nighttime sleep). As  $\chi$  decreases through these regimes ( $\chi\in[0.2,0.41]$ ), similar bifurcations, bistability regimes and disruptions of the  $\rho_{REM}$  period-adding structure take place leading up to the  $\rho=\frac{1}{4}$  solution regime (Fig. 4C). We note that NREM–REM cycling is restricted in the small  $\chi$  limit because the timings of REM activation and REM bout duration do not scale with  $\chi$  and the homeostatic sleep drive time constants, like the timing and duration of sleep episodes in our model. For completeness we discuss how model dynamics and map structure evolve for the three-state model in the small  $\chi$  limit when the growth and decay of sleep need is very fast. However, we do not expect these theoretical results to be representative of actual polyphasic sleep patterns in infants or in other species where REM episodes can be very short.

As  $\chi$  decreases and sleep episodes become shorter, the number of NREM–REM cycles per sleep episode also decreases. The loss of multiple NREM–REM cycles weakens the influence of ultradian cycling on sleep–wake dynamics. For example, the average number of REM bouts

per sleep episode reduces to 1 for  $\chi \in [0.099, 0.226]$ . This encompasses the regime where  $\rho = \frac{1}{4}$  solutions are stable ( $\chi \in [0.205, 0.2185]$ ) suggesting that whenever there are four daily sleep episodes there will be an average of one REM bout per sleep episode. When solutions have only one REM bout per sleep episode, it always occurs at the end of the sleep episode at the transition from the sleep to the wake state. In this way, the timing of the REM bout is constrained within the sleep episode, and the occurrence of REM sleep is influenced primarily by the timing of wake onset. In this  $\chi$  regime, the map becomes continuous, and the gain and loss of stability of the  $\rho = \frac{1}{4}$  solution occurs due to saddle-node bifurcations at  $\chi = 0.2185$  and 0.205, respectively (Fig. 13A,B).

In the two-state model, a significant reduction in the homeostatic time constants also leads to a regime where the map is continuous [29] and no border collision bifurcations can occur. In this continuous regime, the time scale of the homeostatic sleep drive is faster than the time scale of the circadian drive at all phases. Thus, grazing bifurcations that led to discontinuities in the map at phases when the circadian drive was evolving faster than the sleep homeostat, no longer occur. In the Two-Process model, continuous maps were obtained when amplitudes of the circadian threshold curves were decreased [30]. Analysis of these two-state models suggests that once the map becomes continuous, continuity is preserved as model parameters are further varied.

In the three-state model, continuity of the map additionally requires that the number of REM bouts per sleep episode does not differ between distinct sleep episodes. Therefore, although the map becomes continuous at  $\chi=0.224$ , discontinuities can reappear in the map as  $\chi$  is decreased further if the number of REM bouts is no longer

constant across sleep episodes. Here, the map becomes discontinuous again due to the occurrence of sleep episodes with either 1 or 0 REM bouts (Fig. 13C). The transience of the  $\chi$  regime in which the map is continuous in the three-state model contrasts with the preservation of continuity in the maps of two-state models.

### 4. Discussion

In this work, we investigated the influence of NREM–REM alternation on sleep patterns generated by varying homeostatic sleep drive time constants in a sleep—wake network model that simulates three states: wake, NREM sleep, and REM sleep. We found that changing the rates of growth and decay of homeostatic sleep need resulted in a transition between polyphasic and monophasic sleep suggesting that slower accumulation of sleep need is associated with consolidation of sleep into fewer sleep episodes. This finding is consistent with the experimental characterization of the time constants of the sleep homeostat in multiple mammalian species [18,26] and in different human life stages [56–58]. In addition, we found that NREM–REM cycling produced more complicated sequences of bifurcations in the transition between polyphasic to monophasic sleep compared to models with only one sleep state. These findings have implications for understanding the consolidation of sleep in early childhood.

Since the rates of growth and decay of the homeostatic sleep drive modulate the timing and duration of sleep episodes, changes in these rates cause sleep onsets to occur at different circadian phases that then affect the number and duration of REM bouts that occur during the sleep episode. Thus, small differences in homeostatic and circadian modulation can produce large variability in sleep—wake behavior. We characterized this variability using rotation numbers  $\rho$  and  $\rho_{REM}$ ; identification of NREM–REM cycling patterns; and representative circle maps of different orders computed from the sleep—wake network model.

We found that the monotonic change in  $\rho$  observed in two-state models of sleep—wake behavior as homeostatic time constants are varied [26,28,29] is disrupted when the dynamics of NREM–REM cycling are included. Specifically, the three-state model produces more complicated transitions as solutions evolve from monophasic to biphasic sleep patterns, including intervals of bistability, as well as diversity of solutions with varied patterns of NREM–REM cycling across the same number of daily sleep episodes. This suggests that ultradian cycling may interact with developmentally-mediated changes in sleep need to produce a wide range of multi-day sleep patterns and should be considered as part of the underlying dynamics of sleep—wake regulation in early childhood.

### Bifurcations in sleep onset maps

We presented a computationally-based analysis of changes in sleep patterning and investigated the bifurcations that produce these changes using circle maps. Maps were constructed numerically from the highdimensional, physiologically-based sleep-wake regulatory network model for human sleep [31,59]. The maps are non-monotonic and are characterized by multiple discontinuities separating branches that correspond to solutions with distinct NREM-REM cycling patterns. The number of REM bouts associated with each branch was determined by simulating the model from map initial conditions. The particular map structure predicts the transitions in the numbers of average sleep cycles per day as homeostatic time constants are varied. Simultaneously, one can determine the number of REM bouts associated with stable solutions by cobwebbing on the map and tracking which map branches are visited by the solution. Changes in the average number of sleep cycles per day and the associated NREM-REM cycling patterns result from sequences of period doubling, saddle-node and border collision

Specifically, we have shown that in the monophasic sleep ( $\rho = 1$ ) regime, decreasing the homeostatic time constants causes a stable fixed point solution to first lose stability and then lose existence by moving

through a discontinuity of the map. The change in stability of the fixed point occurs in a period-doubling bifurcation leading to the emergence of higher-order periodic solutions with some sleep episodes containing an increased number of REM bouts. As homeostatic time constants are decreased further, saddle–node bifurcations initiate the existence of new stable (and unstable) fixed points with increased numbers of daily REM episodes, and border collisions lead to the destruction of unstable fixed points and higher order cycles. The NREM–REM cycling patterns in the resulting sequence of monophasic sleep solutions display a monotonic period-adding-type increase in the number of daily REM episodes, as quantified by  $\rho_{REM}$ . Additionally, intervals of bistability exist between higher-order periodic solutions and stable fixed point solutions created by saddle–node bifurcations.

Our results show that generally similar bifurcation sequences take place in regimes with multiple sleeps per day ( $\rho$  < 1) as homeostatic time constants decrease. However, NREM-REM cycling can be more variable and the bifurcation sequence does not follow an incremental period-adding type increase in the number of daily REM episodes, as quantified by  $\rho_{REM}$ . Specifically, when multiple daily sleep episodes occur the distribution of the number of REM bouts across the sleep episodes can vary, leading to multiple patterns of NREM-REM cycling exhibiting the same  $\rho_{REM}$  value. Additionally, as we analyzed in detail for biphasic  $(\rho = \frac{1}{2})$  sleep, the number of daily REM bouts can show incremental decreases and incremental increases in different ranges of the homeostatic time constants caused by saddle-node bifurcations and sequences of bifurcations in higher order cycling solutions. Changes in the number of REM bouts produce discontinuous changes in the duration of the overall sleep episode consistent with longitudinal studies of sleep in preschool children [2].

### Contrast with results from two-state sleep-wake models

The Two-Process Model and other physiologically-based models that simulate only two states, wake and sleep, without differentiating between REM and NREM sleep [26,28,29], have also been used to analyze the transition between polyphasic and monophasic sleep patterns, as the homeostatic time constants or an equivalent parameter were varied. As this transition takes place, an underlying period adding structure in the average number of sleep cycles per day was observed. Results in the two-state models suggest a strict monotonic change associated with this structure indicating that napping frequency should decrease monotonically as homeostatic sleep need changes across early childhood.

Circle maps have also been employed in these two-state models to analyze the types of bifurcations associated with the transition between monophasic and polyphasic sleep. In particular, the dynamics of the Two-Process model have been analytically reduced to a onedimensional map that is piecewise smooth and may be monotonic or non-monotonic depending on parameter regimes [28,30,60]. Similarlystructured maps have been computed numerically for other two-state models [29]. However, these maps mainly account for the circadian effect on the timing of sleep onset, which may result in a large time separation of nearby solutions. This phenomenon is reflected in a large discontinuity close to peak values of the circadian rhythm, which is also present in the maps computed for the three state model, e.g at  $\Phi_n \approx 0.5$  for  $\chi = 1$  (Fig. 3). In contrast, maps of the three-state model exhibit additional cusp gaps between map branches for trajectories with distinct numbers of REM bouts. These gaps occur due to the interaction of NREM-REM cycling with the homeostatically regulated transition to the wake state.

Studies in two-state models have reported border collision and saddle—node bifurcations as a mechanism of creating or destroying stable and unstable fixed points in the map and thus, causing the transition in sleep patterning. By contrast, in our three-state model, changes in sleep patterning occur through a nested hierarchy of bifurcations that take place as a result of NREM—REM cycling interacting with changing homeostatic dynamics and include period doubling bifurcations as well

as saddle–node and border collision bifurcations. To our knowledge, period doubling solutions have not been reported in the two-state models. In addition, bistability regularly occurred in the transition between stable solutions, in contrast to two-state models. In our three-state model, the existence of period-doubling and bistability is associated with the increased complexity of the map structure, including non-monotonicity and non-invertibility, caused by differences in NREM–REM cycling at distinct circadian phases.

For example, in the three-state model, a change in the number of REM bouts leads to a change in the duration of the sleep episode and its circadian onset phase. Additionally, the propensity for REM bouts to occur varies with the circadian rhythm [59], consistent with experimental characterizations of REM sleep propensity [19]. Thus, as  $\chi$  varies, the interaction between circadian and homeostatic processes leads to changes in the timing and duration of sleep episodes which, in turn, interact with the NREM-REM cycling dynamics within the sleep episode. The distribution of REM bouts in each sleep episode varies for different values of  $\gamma$ , leading to patterns with different average numbers of REM bouts per sleep episode (i.e., different  $\rho_{REM}$  values), but the same average numbers of sleep cycles per day (i.e., the same  $\rho$ values). Moreover, in some  $\chi$  regimes, we found sleep patterns with the same  $\rho$  and  $\rho_{REM}$  values, but distinct NREM-REM cycling sequences. These sleep patterns highlight developmentally-mediated changes in sleep architecture that are not detected when considering  $\rho$  values only but that affect the underlying structure that governs transitions in  $\rho$ . Future work may investigate how circle maps change as the occurrence of REM bouts is reduced (e.g., when the activation threshold for the REM-promoting population is increased [47]).

### Napping, light exposure, and the circadian modulation of sleep

In our analysis, the map construction requires that we assume a fixed light:dark schedule in order to maintain a rigorous definition of circadian phase. However, the light exposure of most humans does not occur at a constant intensity and is not strictly dependent on the environmental light cycle. Instead, individuals experience a wide range of light intensities, and artificial light enables a significant level of self-selection in light exposure that may result in variable daily schedules of both light exposure and sleep—wake behavior [61–63]. In addition, the behavioral gating of light that occurs when eyes are closed during sleep gives rise to feedback between sleep timing and light input to the circadian clock, which may then affect circadian phase. Thus, as the need for naps decreases and children start dropping naps, both their sleep patterns and their patterns of light exposure are affected.

Our modeling approach can incorporate the effect of external light schedules on sleep timing during the transition between polyphasic and monophasic sleep through the light forcing term in the circadian clock model component. Variable patterns of light exposure induce variability in sleep timing reflected in quasi-stable model solutions. However, regular changes in the pattern of light exposure may affect the circadian waveform in a way that reinforces patterns of sleep—wake behavior. In previous work we have shown that the map maintains a good approximation of the dynamics of the full model even when behaviorally-gated light input is included [45]. Thus, we expect that results reported here are qualitatively similar to those that would be obtained if light:dark schedules were allowed to vary with simulated behavioral state. However, more work is needed to establish how interactions between changes in light exposure associated with changing sleep—wake patterns interact with the circadian system.

In addition, REM sleep may represent an indirect pathway for circadian modulation of sleep—wake behavior. In adults, REM sleep is gated by the circadian system [19], but circadian and other features of REM sleep differ across species and in humans at different life stages [17,64–66]. Developmentally-mediated changes in circadian regulation of REM sleep may interact with other developmentally-mediated changes in sleep in early childhood.

Implications and future considerations

REM sleep is a key feature of sleep architecture, and there is evidence that ultradian alternation between NREM and REM sleep interacts with developmental changes in sleep in preschool children [2]. Thus, the presence of unique features in the bifurcation patterns of three-state models (e.g., higher order patterns and bistability) suggests that there may be important aspects of the transition between polyphasic and monophasic sleep that are not captured by two-state models.

The reciprocal interaction hypothesis we incorporated to capture the REM sleep dynamics is one of multiple proposed mechanisms for the generation of NREM–REM alternation [67–71]. However, the interactions between the limit cycle producing ultradian NREM–REM cycling and the hysteresis loop driving transitions between sleep and wake behavior are the distinguishing dynamical features of our three-state model. Therefore, future work should consider the effects of NREM–REM alternation on the transition from polyphasic to monophasic sleep in models that incorporate alternative theories of REM sleep regulation [70–72].

In addition, future experimental work is needed to assess model predictions and provide physiological constraints for model parameters by characterizing concurrent changes in REM sleep and the dynamics of homeostatic sleep need across qualitative transitions in sleep—wake behavior. Changes in homeostatic time constants may not occur uniformly for the increase and dissipation of sleep need [14], and the effects of such non-uniform changes on the transition from polyphasic to monophasic sleep are unknown. Future modeling work investigating the independent and relative contributions of homeostatic and circadian factors in sleep consolidation would complement ongoing experimental studies of sleep across development.

### Declaration of competing interest

The authors declare that they have no known competing financial interests or personal relationships that could have appeared to influence the work reported in this paper.

### Acknowledgments

The authors acknowledge the contribution of Grace O'Brien in generating Fig. 2. The authors also wish to thank Dr. Monique LeBourgeois for helpful conversations about sleep behavior across early childhood and to acknowledge discussions at the "What is Sleep?" working group hosted at the Santa Fe Institute (Santa Fe, NM) in November 2019 that contributed to the ideas in this article.

### Appendix A. Supplementary data

Supplementary material related to this article can be found online at https://doi.org/10.1016/j.mbs.2022.108929.

### References

- E. Aserinsky, N. Kleitman, Regularly occurring periods of eye motility, and concomitant phenomena, during sleep, Science 118 (3062) (1953) 273–274, http: //dx.doi.org/10.1126/science.118.3062.273, arXiv:https://www.science.org/doi/ pdf/10.1126/science.118.3062.273, URL https://www.science.org/doi/abs/10. 1126/science.118.3062.273.
- [2] S. Lopp, W. Navidi, P. Achermann, M. LeBourgeois, C. Diniz Behn, Developmental changes in ultradian sleep cycles across early childhood: Preliminary insights, J. Biol. Rhythms 32 (1) (2017) 64–74, http://dx.doi.org/10.1177/0748730416685451, arXiv:https://doi.org/10.1177/0748730416685451, PMID: 28088873
- [3] C.B. Saper, T.C. Chou, T.E. Scammell, The sleep switch: hypothalamic control of sleep and wakefulness, Trends Neurosci. 24 (2001) 726–731.
- [4] C.B. Saper, T.E. Scammell, J. Lu, Hypothalamic regulation of sleep and circadian rhythms, Nature 437 (2005) 1257–1263.
- [5] R.E. Mistlberger, Circadian regulation of sleep in mammals: role of the suprachiasmatic nucleus, Brain Res. Rev. 49 (2005) 429–454.

- [6] J.H. Meijer, K. Watanabe, J. Schaap, H. Albus, L. Détári, Light responsiveness of the suprachiasmatic nucleus: Long-term multiunit and single-unit recordings in freely moving rats, J. Neurosci. 18 (21) (1998) 9078–9087, http://dx.doi.org/10. 1523/JNEUROSCI.18-21-09078.1998, arXiv:https://www.jneurosci.org/content/ 18/21/9078.full.pdf, URL https://www.jneurosci.org/content/18/21/9078.
- [7] D.K. Welsh, D.E. Logothetis, M. Meister, S.M. Reppert, Individual neurons dissociated from rat suprachiasmatic nucleus express independently phased circadian firing rhythms, Neuron 14 (4) (1995) 697–706, http://dx.doi.org/10.1016/ 0896-6273(95)90214-7, URL https://www.sciencedirect.com/science/article/pii/ 0896627395902147.
- [8] R. Basheer, R. Strecker, M. Thakkar, R. McCarley, Adenosine and sleep-wake regulation, Prog. Neurobiol. 73 (2004) 379–396.
- [9] Z. Huang, Y. Urade, O. Hayaishi, Prostaglandins and adenosine in the regulation of sleep and wakefulness, Curr. Opin. Pharmacol. 7 (2007) 33–38.
- [10] T. Tekieh, P.A. Robinson, S. Postnova, Cortical waste clearance in normal and restricted sleep with potential runaway tau buildup in Alzheimer's disease, Sci. Rep. 12 (2022).
- [11] D.J. Dijk, D.G.M. Beersma, S. Daan, EEG power density during nap sleep: Reflection of an hourglass measuring the duration of prior wakefulness, J. Biol. Rhythms 2 (3) (1987) 207–219, http://dx.doi.org/10. 1177/074873048700200304, arXiv:https://doi.org/10.1177/0748730487002003 04, PMID: 2979661.
- [12] S. Daan, D. Beersma, A. Borbely, Timing of human sleep: recovery process gated by a circadian pacemaker, Am. J. Physiol.-Regul. Integr. Comp. Physiol. 246 (1984) R161–R183.
- [13] T. Rusterholz, R. Durr, P. Achermann, Inter-individual differences in the dynamics of sleep homeostasis, SLEEP 33 (2010) 491–498.
- [14] O. Jenni, P. Achermann, M. Carskadon, Homeostatic sleep regulation in adolescents, SLEEP 28 (2005) 1446–1454.
- [15] D. Aeschbach, C. Cajochen, H. Landolt, A.A. Borbely, Homeostatic sleep regulation in habitual short sleepers and long sleepers, Am. J. Physiol.-Regul. Integr. Comp. Physiol. 270 (1) (1996) R41–R53, http://dx.doi.org/10.1152/ajpregu.1996.270.1.R41, arXiv:https://doi.org/10.1152/ajpregu.1996.270.1.R41, PMID: 8769783.
- [16] M. LeBourgeois, T. Rusterholz, O. Jenni, M. Carskadon, P. Achermann, Do the dynamics of sleep homeostasis (process S) change across early childhood? in: Presented At the 26th Annual Meeting of the Associated Professional Sleep Societies (APSS), Boston, MA, USA, 9–13 June 2012. Abstract 0050.
- [17] I. Tobler, Is sleep fundamentally different between mammalian species? Behav. Brain Res. 69 (1995) 35–41.
- [18] I. Tobler, P. Franken, L. Trachsel, A. Borbely, Models of sleep regulation in mammals, J. Sleep Res. 1 (1992) 125–127.
- [19] C.A. Czeisler, J.C. Zimmerman, J.M. Ronda, M.C. Moore-Ede, E.D. Weitzman, Timing of REM sleep is coupled to the circadian rhythm of body temperature in man, Sleep 2 (3) (1980) 329–346, http://dx.doi.org/10.1093/sleep/2.3.329.
- [20] D.-J. Dijk, C.A. Czeisler, Contribution of the circadian pacemaker and the sleep homeostat to sleep propensity, sleep structure, electroencephalographic slow waves, and sleep spindle activity in humans, J. Neurosci. 15 (1995) 3526–3538.
- [21] A. Ocampo-Garcés, A. Bassi, E. Brunetti, J. Estrada, E.A. Vivaldi, REM sleep-dependent short-term and long-term hourglass processes in the ultradian organization and recovery of REM sleep in the rat, Sleep 43 (8) (2020) http://dx.doi.org/10.1093/sleep/zsaa023, arXiv:https://academic.oup.com/sleep/article-pdf/43/8/zsaa023/33641006/zsaa023.pdf, zsaa023.
- [22] S.H. Piltz, C.G. Diniz Behn, V. Booth, Habitual sleep duration affects recovery from acute sleep deprivation: A modeling study, J. Theoret. Biol. 504 (2020) 110401, http://dx.doi.org/10.1016/j.jtbi.2020.110401, URL https://www.sciencedirect.com/science/article/pii/S0022519320302563.
- [23] O. Benoit, J. Foret, G. Bouard, B. Merle, J. Landau, M. Marc, Habitual sleep length and patterns of recovery sleep after 24 hour and 36 hour sleep deprivation, Electroencephalogr. Clin. Neurophysiol. 50 (5) (1980) 477–485, http: //dx.doi.org/10.1016/0013-4694(80)90014-0, URL https://www.sciencedirect. com/science/article/pii/0013469480900140.
- [24] M. Carskadon, W. Dement, Normal human sleep: an overview, in: M. Kryger, T. Roth, W. Dement (Eds.), Principles and Practice of Sleep Medicine, Elsevier Saunders, St. Louis, 2011.
- [25] H. Gaudreau, J. Carrier, J. Montplaisir, Age-related modifications of NREM sleep EEG: from childhood to middle age, J. Sleep Res. 10 (2001) 165–172.
- [26] A.J.K. Phillips, B.D. Fulcher, P.A. Robinson, E.B. Klerman, Mammalian rest/activity patterns explained by physiologically based modeling, PLoS Comput. Biol. 9 (9) (2013) http://dx.doi.org/10.1371/journal.pcbi.1003213.
- [27] R. Allada, J.M. Siegel, Unearthing the phylogenetic roots of sleep, Curr. Biol. 18 (15) (2008) R670–R679, http://dx.doi.org/10.1016/j.cub.2008.06.033, URL https://www.sciencedirect.com/science/article/pii/S0960982208007550.
- [28] A. Skeldon, D.-J. Dijk, G. Derks, Mathematical models for sleep-wake dynamics: Comparison of the two-process model and a mutual inhibition neuronal model, PLoS One 9 (2014) e103877.
- [29] C. Athanasouli, S.H. Piltz, C.G. Diniz Behn, V. Booth, Bifurcations of sleep patterns due to homeostatic and circadian variation in a sleep-wake flip-flop model, SIAM J. Appl. Dyn. Syst. 21 (3) (2022) 1893–1929, http://dx.doi.org/ 10.1137/21M1446149, arXiv:https://doi.org/10.1137/21M1446149.

- [30] M.P. Bailey, G. Derks, A.C. Skeldon, Circle maps with gaps: Understanding the dynamics of the two-process model for sleep-wake regulation, European J. Appl. Math. 29 (5) (2018) 845–868, http://dx.doi.org/10.1017/S0956792518000190.
- [31] V. Booth, I. Xique, C.G. Diniz Behn, One-dimensional map for the circadian modulation of sleep in a sleep-wake regulatory network model for human sleep, SIAM J. Appl. Dyn. Syst. 16 (2017) 1089–1112.
- [32] C. Diniz Behn, V. Booth, Simulating microinjection experiments in a novel model of the rat sleep-wake regulatory network, J. Neurophysiol. 103 (2010) 1937–1953.
- [33] M. Fleshner, V. Booth, D. Forger, C. Diniz Behn, Circadian regulation of sleepwake behavior in nocturnal rats requires multiple signals from suprachiasmatic nucleus, Phil. Trans. R. Soc. A 369 (2011) 3855–3883.
- [34] J. Hobson, R. McCarley, P. Wyzinski, Sleep cycle oscillation: reciprocal discharge by two brainstem neuronal groups, Science 189 (4196) (1975) 55–58, http://dx.doi.org/10.1126/science.1094539, arXiv:https://science. sciencemag.org/content/189/4196/55.full.pdf, URL https://science.sciencemag. org/content/189/4196/55.
- [35] T. Porkka-Heiskanen, R.E. Strecker, M. Thakkar, A.A. Bjørkum, R.W. Greene, R.W. McCarley, Adenosine: A mediator of the sleep-inducing effects of prolonged wakefulness, Science 276 (5316) (1997) 1265–1268, http://dx.doi.org/10.1126/science.276.5316.1265, arXiv:https://www.science.org/doi/pdf/10.1126/science.276.5316.1265, URL https://www.science.org/doi/abs/10.1126/science.276.5316.1265.
- [36] T. Porkka-Heiskanen, R. Strecker, R. McCarley, Brain site-specificity of extracellular adenosine concentration changes during sleep deprivation and spontaneous sleep: an in vivo microdialysis study, Neuroscience 99 (3) (2000) 507–517, http://dx.doi.org/10.1016/S0306-4522(00)00220-7, URL https://www.sciencedirect.com/science/article/pii/S0306452200002207.
- [37] N. Chamberlin, E. Arrigoni, T. Chou, T. Scammell, R. Greene, C. Saper, Effects of adenosine on gabaergic synaptic inputs to identified ventrolateral preoptic neurons, Neuroscience 119 (4) (2003) 913–918, http://dx.doi.org/ 10.1016/S0306-4522(03)00246-X, URL https://www.sciencedirect.com/science/ article/pii/S030645220300246X.
- [38] S. Morairty, D. Rainnie, R. McCarley, R. Greene, Disinhibition of ventrolateral preoptic area sleep-active neurons by adenosine: a new mechanism for sleep promotion, Neuroscience 123 (2) (2004) 451–457, http://dx.doi.org/10.1016/ j.neuroscience.2003.08.066, URL https://www.sciencedirect.com/science/article/ pii/S0306452203006705.
- [39] G. Deco, V.K. Jirsa, P.A. Robinson, M. Breakspear, K. Friston, The dynamic brain: from spiking neurons to neural masses and cortical fields, PLoS Comput. Biol. 4 (2008) e1000092.
- [40] A.J.K. Phillips, C.A. Czeisler, E.B. Klerman, Revisiting spontaneous internal desynchrony using a quantitative model of sleep physiology, J. Biol. Rhythms 26 (2011) 441–453.
- [41] V. Booth, C.G. Diniz Behn, Physiologically-based modeling of sleep/wake regulatory networks, Math. Biosci. 250 (2014) 54–68.
- [42] H.R. Wilson, J.D. Cowan, Excitatory and inhibitory interactions in localized populations of model neurons, Biophys. J. 12 (1972) 1–24.
- [43] D.B. Forger, M.E. Jewett, R.E. Kronauer, A simpler model of the human circadian pacemaker, J. Biol. Rhythms 14 (1999) 532–537.
- [44] D.B. Forger, Biological Clocks, Rhythms, and Oscillations: The Theory of Biological Timekeeping, MIT Press, 2017.
- [45] S.H. Piltz, C. Athanasouli, C.G. Diniz Behn, V. Booth, Mapping recovery from sleep deprivation, Commun. Nonlinear Sci. Numer. Simul. 96 (2021) 105686, http://dx.doi.org/10.1016/j.cnsns.2020.105686, URL https://www.sciencedirect. com/science/article/pii/S1007570420305165.
- [46] G.B. Ermentrout, Simulating, Analyzing, and Animating Dynamical Systems: A Guide To XPPAUT for Researchers and Students, Society for Industrial and Applied Mathematics, Philadelphia, 2002.
- [47] C. Diniz Behn, V. Booth, A fast-slow analysis of the dynamics of REM sleep, SIAM J. Appl. Dyn. Syst. 11 (2012) 212–242.
- [48] S.H. Strogatz, Nonlinear Dynamics and Chaos: With Applications to Physics, Biology, Chemistry, and Engineering, Second ed., in: Studies in Nonlinearity, CRC Press, 2018.
- [49] M. di Bernardo, C.J. Budd, A.R. Champneys, Normal form maps for grazing bifurcations in n-dimensional piecewise-smooth dynamical systems, Physica D 160 (2001) 222–254.
- [50] V. Avrutin, L. Gardini, I. Sushko, F. Tramontana, Continuous and Discontinuous Piecewise-Smooth One-Dimensional Maps, WORLD SCIENTIFIC, 2019, http://dx.doi.org/10.1142/8285, arXiv:https://www.worldscientific.com/doi/pdf/10.1142/8285, URL https://www.worldscientific.com/doi/abs/10.1142/8285.
- [51] J.P. Keener, L. Glass, Global bifurcations of a periodically forced nonlinear oscillator, J. Math. Biol. 21 (2) (1984) 175–190, http://dx.doi.org/10.1007/ BF00277669.
- [52] S. Staton, P.S. Rankin, M. Harding, S.S. Smith, E. Westwood, M.K. LeBourgeois, K.J. Thorpe, Many naps, one nap, none: A systematic review and meta-analysis of napping patterns in children 0–12 years, Sleep Med. Rev. 50 (2020) 101247, http://dx.doi.org/10.1016/j.smrv.2019.101247, URL https://www.sciencedirect. com/science/article/pii/S1087079219302151.

- [53] H.C. Gustafsson, C.B. Propper, Developmental trajectories of toddler sleep problems: can a person-centered approach help identify children at risk? Sleep (2022) http://dx.doi.org/10.1093/sleep/zsac142, arXiv:https://academic.oup.com/sleep/advance-article-pdf/doi/10.1093/sleep/zsac142/44724605/zsac142.pdf, zsac142.
- [54] L.D. Akacem, C.T. Simpkin, M.A. Carskadon, K.P. Wright Jr., O.G. Jenni, P. Achermann, M.K. LeBourgeois, The timing of the circadian clock and sleep differ between napping and non-napping toddlers, PLOS ONE 10 (4) (2015) 1–12, http://dx.doi.org/10.1371/journal.pone.0125181.
- [55] M. LeBourgeois, T. Rusterholtz, O. Jenni, M. Carskadon, P. Achermann, Do the dynamics of sleep homeostasis (process S) change across early childhood? in: SLEEP, Vol. 35, 2012, p. A21.
- [56] C. Acebo, A. Sadeh, R. Seifer, O. Tzischinsky, A. Hafer, M. Carskadon, Sleep/wake patterns derived from activity monitoring and maternal report for healthy 1- to 5-year old children, Sleep 28 (2005) 1568–1577.
- [57] I. Iglowstein, O. Jenni, L. Molinari, R. Largo, Sleep duration from infancy to adolescence: reference values and generational trends, Pediatrics 111 (2003) 302–307
- [58] O. Jenni, M. LeBourgeois, Understanding sleep-wake behavior and sleep disorders in children: the value of a model, Curr. Opin. Psychiatry 19 (2006) 282–287.
- [59] R.D. Gleit, C. Diniz Behn, V. Booth, Modeling interindividual differences in spontaneous internal desynchrony patterns, J. Biol. Rhythms 28 (2013) 339–355.
- [60] M. Nakao, H. Sakai, M. Yamamoto, An interpretation of the internal desynchronizations based on dynamics of the two-process model, Methods Inf. Med. 36 (1997) 282–285.
- [61] A.C. Skeldon, A.J.K. Phillips, D.-J. Dijk, The effects of self-selected light-dark cycles and social constraints on human sleep and circadian timing: a modeling approach, Sci. Rep. 7 (2017) 45158 EP.
- [62] E.R. Stothard, A.W. McHill, C.M. Depner, B.R. Birks, T.M. Moehlman, H.K. Ritchie, J.R. Guzzetti, E.D. Chinoy, M.K. LeBourgeois, J. Axelsson, K.P. Wright, Circadian entrainment to the natural light-dark cycle across seasons and the weekend, Curr. Biol. 27 (4) (2017) 508–513, http://dx.doi.org/10.1016/j.cub. 2016.12.041

- [63] A. Martinez-Nicolas, E. Ortiz-Tudela, J.A. Madrid, M.A. Rol, Crosstalk between environmental light and internal time in humans, Chronobiol. Int. 28 (7) (2011) 617–629.
- [64] M. Ohayon, M. Carskadon, C. Guilleminault, M. Vitiello, Meta-analysis of quantiative sleep parameters from childhood to old age in healthy individuals: developing normative sleep values across the human lifespan, SLEEP 27 (2004) 1255–1273.
- [65] J. Siegel, REM sleep, in: M. Kryger, T. Roth, W. Dement (Eds.), Principles and Practice of Sleep Medicine, Elsevier Saunders, St. Louis, 2011.
- [66] J. Cao, A.B. Herman, G.B. West, G. Poe, V.M. Savage, Unraveling why we sleep: Quantitative analysis reveals abrupt transition from neural reorganization to repair in early development, Sci. Adv. 6 (38) (2020) eaba0398, http://dx.doi. org/10.1126/sciadv.aba0398, arXiv:https://www.science.org/doi/pdf/10.1126/ sciadv.aba0398, URL https://www.science.org/doi/abs/10.1126/sciadv.aba0398.
- [67] R.W. McCarley, J.A. Hobson, Neuronal excitability modulation over the sleep cycle: a structural and mathematical model, Science 189 (1975) 58–60.
- [68] Y.-Q. Wang, W.-Y. Liu, L. Li, W.-M. Qu, Z.-L. Huang, Neural circuitry underlying REM sleep: A review of the literature and current concepts, Prog. Neurobiol. 204 (2021) 102106, http://dx.doi.org/10.1016/j.pneurobio.2021.102106, URL https://www.sciencedirect.com/science/article/pii/S0301008221001209.
- [69] J. Lu, D. Sherman, M. Devor, C.B. Saper, A putative flip-flop switch for control of REM sleep, Nature 441 (2006) 589–594.
- [70] O. Le Bon, Relationships between REM and NREM in the NREM-REM sleep cycle: a review on competing concepts, Sleep Med. 70 (2020) 6–16, http: //dx.doi.org/10.1016/j.sleep.2020.02.004, URL https://www.sciencedirect.com/ science/article/pii/S1389945720300757.
- [71] F. Weber, Modeling the mammalian sleep cycle, Curr. Opin. Neurobiol. 46 (2017) 68–75, http://dx.doi.org/10.1016/j.conb.2017.07.009, URL https://www.sciencedirect.com/science/article/pii/S095943881730020X. Computational Neuroscience.
- [72] O.L. Bon, An asymmetrical hypothesis for the NREM-REM sleep alternation—what is the NREM-REM cycle? Front. Neurosci. 15 (2021) http://dx.doi.org/10.3389/fnins.2021.627193.